Adaptive Control of a Farm Tractor with Varying Yaw Properties

Accounting for Actuator Dynamics and Nonlinearities

Except where reference is made to the work of others, the work described in this thesis is my own or was done in collaboration with my advisory committee. This thesis does not include proprietary or classified information.

J. Benton Derrick

Certificate of Approval:

George T. Flowers Professor Mechanical Engineering	David M. Bevly, Chair Associate Professor Mechanical Engineering
John Y. Hung Professor Electrical and Computer Engineering	Joe F. Pittman Interim Dean Graduate School

Adaptive Control of a Farm Tractor with Varying Yaw Properties Accounting for Actuator Dynamics and Nonlinearities

J. Benton Derrick

A Thesis

Submitted to

the Graduate Faculty of

Auburn University

in Partial Fulfillment of the

Requirements for the

Degree of

Master of Science

Auburn, Alabama
May 10, 2008

Adaptive Control of a Farm Tractor with Varying Yaw Properties

Accounting for Actuator Dynamics and Nonlinearities

J. Benton Derrick

_____

Signature of Author

_____

Date of Graduation

Vita

J. Benton Derrick was born in Rome, GA, on April 24, 1984. He is the second child of David and Rebecca and brother to Jennifer. He was raised in Centre, AL, and attended Centre Elementary School, Centre Middle School, and Cherokee County High School. Upon graduation from high school in 2002, He attended Auburn University and completed his bachelor of mechanical engineering degree in the spring of 2006. He then accepted a graduate research assistant position in the Global Positioning System and Vehicle Dynamics Laboratory the following summer to work on a masters of science degree with specialization in dynamics and controls. Benton was wed to Vanessa Attaway in January of 2007.

Thesis Abstract

Adaptive Control of a Farm Tractor with Varying Yaw Properties Accounting for Actuator Dynamics and Nonlinearities

J. Benton Derrick

Master of Science, May 10, 2008
(B.M.E., Auburn University, 2006)

112 Typed Pages

Directed by David M. Bevly

Two adaptive control algorithms for the automatic steering control of a farm tractor with varying hitch forces are developed. Tractors can be configured many different implements, and implements interact with the soil in various ways. These variations cause the yaw dynamics to change with respect to different implements and soil conditions; therefore, this thesis uses a model reference adaptive (MRAC) control law to compensate for different implement configurations. Models are described and analyzed for the steering actuator, yaw rate plant, and lateral position plant. It is shown that the DC gain of the steering angle to yaw rate transfer function is the model parameter that changes the most with hitch loading. In order to develop the adaptive control algorithm, a cascaded controller is first implemented with three feedback loops containing the steering angle, yaw rate, and lateral position measurements. Controllers are designed for each subsystem, and root locus analysis is used to describe the stability and performance characteristics.

Two MRAC algorithms are derived to compensate the loop gain and feed-forward gain of the yaw rate controller to account for changes in the yaw rate plant. The two algorithms are named the model reference adaptive control loop gain adaptation (MRAC-LGA) algorithm and the model reference adaptive control feed-forward gain adaptation (MRAC-FGA) algorithm. Simulations are presented that show that the algorithms perform poorly due to neglected steering actuator properties. Both algorithms are modified to account for the steering actuator properties, and more simulations are presented that demonstrate satisfactory performance. Experimental results are presented for the LGA algorithm, and issues with experimental implementation are discussed. Next, experimental results are presented for the FGA algorithm that show improved performance over the LGA algorithm. Finally, experimental tests further validate that the FGA algorithm improves lateral error performance versus a fixed-gain controller.

Acknowledgments

I would first like to thank God for my strength and wisdom that he gives me. I am truly blessed with all of the opportunity that has be afforded me. I next thank my wife Vanessa for her love, patience, support and allowing me to put our life on hold while I pursue my education. I also would like to thank my parents for their love and support throughout my entire life. I would not be where I am today if it was not for them. Thanks goes to Professor David Bevly for his guidance and assistance during my tenure in the GAVLAB and for giving me a chance to earn my master's degree while working on exciting projects. I would finally like to thank all of the members of the GAVLAB for their assistance and comradery over the last couple of years.

Style manual or journal used Journal of Approximation Theory (together with the style known as "aums"). Bibliography follows van Leunen's *A Handbook for Scholars*.

Computer software used The document preparation package TEX (specifically LATEX) together with the departmental style-file `aums.sty`.

Table of Contents

List of Figures

List of Tables

Chapter 1

Introduction

1.1 Motivation

Automatically steered farm tractors have become popular in the last few years due to the advantages that they bring farmers. Advances in Global Positioning System (GPS) technology has created a means to measure the position of a user within 2 cm [Montgomery, 1996]. This accuracy has allowed precision farming to flourish. Many problems such as overlap, driver inexperience, poor visibility, in-ground irrigation destruction, and crop destruction can be addressed with automatically steered farm tractors. Figure 1.1 shows a field that has been plowed using an automatically steered farm tractor. Notice that the rows are nearly perfectly straight.

Figure 1.1: Field Bedded for Planting with Automatically Steered Tractor

Farm tractors can be outfitted with a variety of attachments that can change the forces that are applied to the hitch. Additionally, different soil conditions can

be encountered that will make the same implement have different force properties. Because the hitch force response changes, the yaw rate response changes as well. It is desired that the response of the tractor be as consistent as possible. A fixed-gain controller designed for a time-invariant plant has the potential for poor performance and unstable characteristics.

On current John Deere production models, there is a sensitivity parameter that has to be field tuned by the user. The adjustment parameter effectively scales the steering angle of the tractor by a gain. There are many problems with this method. First, the sensitivity parameter is often poorly tuned. The poorly tuned gain causes oscillation of the tractor or undue lateral position error. Since the sensitivity parameter is a fixed value, the tractor will often exhibit unstable behavior while the implement is out of the ground when the system is tuned for big implements. Also, there is no way for the sensitivity parameter to be adjusted to account for changing soil conditions other than by the operator stopping the tractor and manually changing the gain. An example of this behavior is shown in Figure 1.2. The tractor was started with the implement deep in the ground, and then the implement was lifted up at the specified point in time. Notice that there is significantly more lateral error after the implement is lifted our of the ground. For all these reasons, having a fixed sensitivity parameter is not a good solution.

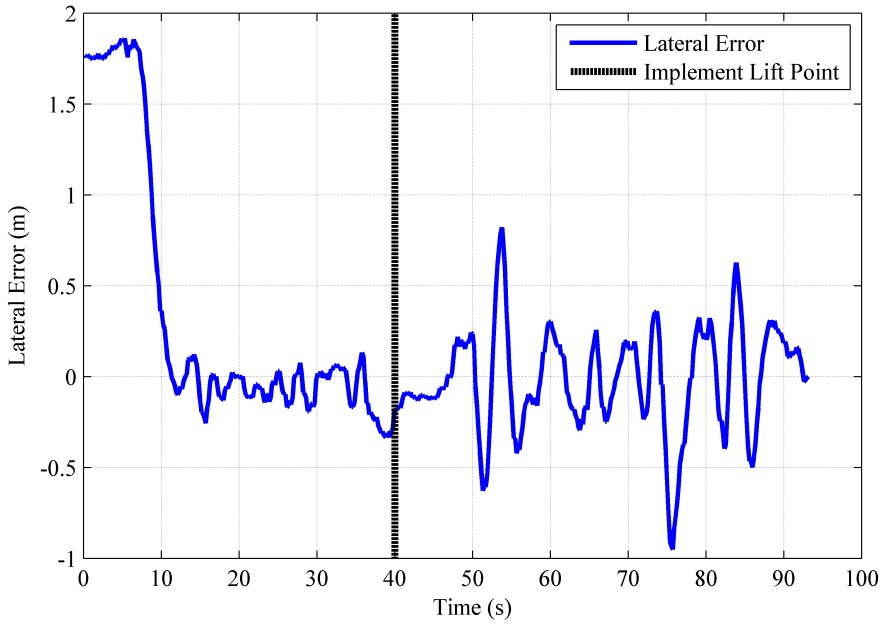

Figure 1.2: Lateral Position Response with Implement Lifted Out of Ground

It is desired to make the sensitivity parameter automatically adjust to different implements, depths, and soil conditions by a direct adaptive control approach. The focus of this thesis will be on developing an adaptive control algorithm to directly adjust the sensitivity parameter of the yaw rate controller.

1.2 Background and Prior Work

Work has been previously completed on modeling, control, and estimation of farm tractor dynamics with implements. The first work of modeling a farm tractor with an implement was [O'Conner, 1997]. This work took the Wong bicycle model and augmented the implement forces onto the rear of the tractor [Wong, 1978]. The implement forces were modeled as an extra axle behind the rear axle, and

the lateral axle force is proportional to the slip angle between the velocity vector and the heading angle of the axle. There have been numerous implement-soil mechanics models developed, but these models only predict the longitudinal and vertical forces [R. Berntsen and Aasen, 2006], [Godwin and O'Dogherty, 2007], [Rosa and Wulfsohn, 1999], [Sahu and Raheman, 2006]. Since the lateral forces of the implement are what influence the yaw rate dynamics, the bicycle model with the third axle is the best model available to predict yaw dynamics of a tractor with a hitched implement. This model was shown to be valid for implements attached to the tractor using the three-point hitch [Pearson, 2007]. Simulations have also been complemented on tractor-implement interactions for implements that are attached to the draw bar hitch of the tractor [Pota, 2007].

In the more general field of modeling and controlling farm tractors, many other works have been completed. Work has been completed on modeling high-speed ground vehicles using tire relaxation lengths [Bevly, 2001]. A farm tractor has been controlled using only a single carrier phase differential global positioning system (CP-DGPS) receiver [Thuilot and Berducat, 2002]. Also, a farm tractor has been controlled using vision based navigation [Zolton, 1998].

Because the implement forces cause the yaw rate dynamics to vary, there have been studies completed to adapt the lateral position controller to account for this variation. One work used estimation algorithms such as least mean squares and the Kalman filter to estimate yaw model parameters [Rekow, 2001]. Another work used an extended Kalman filter to estimate the slope of the DC gain of the steering angle

to yaw rate transfer function with respect to velocity [Gartley and Bevly, 2005] . In both cases, the estimated parameters were used to indirectly adapt the lateral position controller.

There have been other research completed on adaptive control of ground vehicles. A model reference adaptive control (MRAC) system has been implemented on a vehicle to create an active steering control system [Fukao, 2001]. Also, a vehicle guidance controller has been adapted using a form of MRAC [Hessburg, 1995]. There has also been a gain scheduling approach to active steering using a form of the bicycle model [Baslamish, 2007].

MRAC systems first came into existence during the middle of the 20th century. The original theory was applied to controlling airplanes that have varying loads and aerodynamic properties [Whitaker and Kezer, 1958]. The fundamental idea behind MRAC systems is to create a controller update law that will adjust controller parameters so that the plant output matches a desired model output [Astrom and Wittenmark, 1995]. The MIT rule was the first approach to MRAC, and it was widely accepted for its straight-forward application.

1.3 Contributions

This thesis presents a novel application of model reference adaptive control theory on an automatically steered farm tractor. In development of this control application, the following specific tasks were performed:

- A cascaded controller was designed to control the lateral position of the farm tractor.
- A MRAC system was designed to compensate for yaw plant variations by adapting the loop gain of the yaw rate controller called the MRAC-LGA algorithm.
- A MRAC system was designed to compensate for yaw plant variations by adapting the feed-forward yaw rate controller called the MRAC-FGA algorithm.
- Both MRAC algorithms were modified to account for steering actuator dynamics and nonlinearities.
- The MRAC system was implemented experimentally and was shown to outperform a fixed-gain controller.

1.4 Outline of Thesis

In Chapter 2, models are described and analyzed for the steering actuator, yaw rate plant, and lateral position plant. It is shown that the DC gain of the

steering angle to yaw rate transfer function is the model parameter that changes the most with hitch loading. A cascaded controller is implemented with three feedback loops containing the steering angle, yaw rate, and lateral position measurements. Controllers are designed for each subsystem, and root locus analysis is used to describe the stability and performance characteristics.

A MRAC algorithm is developed in Chapter 3 to adapt the loop gain of the yaw rate control system to account for the changing yaw rate plant parameters. Simulation results are presented to show the performance of the MRAC system, and modifications are made to the algorithm to account for the steering actuator dynamics and nonlinearities. Finally, the algorithm is implemented on a John Deere 8420, and experimental results are presented. Some issues are presented describing the short comings of the algorithm.

In Chapter 4, another MRAC algorithm is designed to address the issues that came from adapting the loop gain. A feed-forward yaw rate controller is added to the system, and this will be adapted to account for changing yaw dynamics. Simulations are again presented that show the performance of the new algorithm. Experimental results are presented that show the performance under a step input. Finally, the lateral error characteristics of the algorithm are compared to a fixed-gain configuration.

Chapter 2

System Models and Control Architecture

2.1 Introduction

This chapter presents the system models, controller architecture, and controller design used in this thesis. Three different subsystems are combined to regulate the lateral position of the farm tractor: the steering actuator, yaw rate plant, and lateral position plant. A model and controller is presented and analyzed for each subsystem. The steering actuator model is derived from system identification experiments performed previously by [Gartley, 2005]. The steering actuator subsystem contains nonlinearities that are accounted for by an inversion lookup table. A linear model of the actuator is then presented combining the lookup table and dynamic model. The presented yaw rate dynamic model is from work by [Pearson and Bevly, 2005] and [O'Conner, 1997]. The yaw rate dynamic model is a derivation of a bicycle model augmented with a third axle at the rear of the tractor. Analysis is performed on the model in simulation which describes how the model varies with hitch loading to provide basis for adaptive control. A kinematic model of the lateral position plant is then presented. Finally, the controllers of the subsystems are presented and analyzed.

2.2 System Modeling

2.2.1 Steering Actuator Model

The steering actuator on the John Deere 8420 is a hydraulic cylinder that is controlled through the controller area network (CAN) bus on the farm tractor. The hydraulic valve of the steering actuator is commanded at 50 Hz by sending a counts value that corresponds to a desired flow. The flow through the valve is proportional to the steering angle slew rate. Previous research has been completed on identifying the steering actuator dynamics and nonlinearities [Gartley, 2005]. Figure 2.1 shows the input to output characteristics of the steering actuator. As can be seen, there is deadband, saturations, and nonlinearities. The curve fits of each region of the steering calibration are shown in Table 2.1.

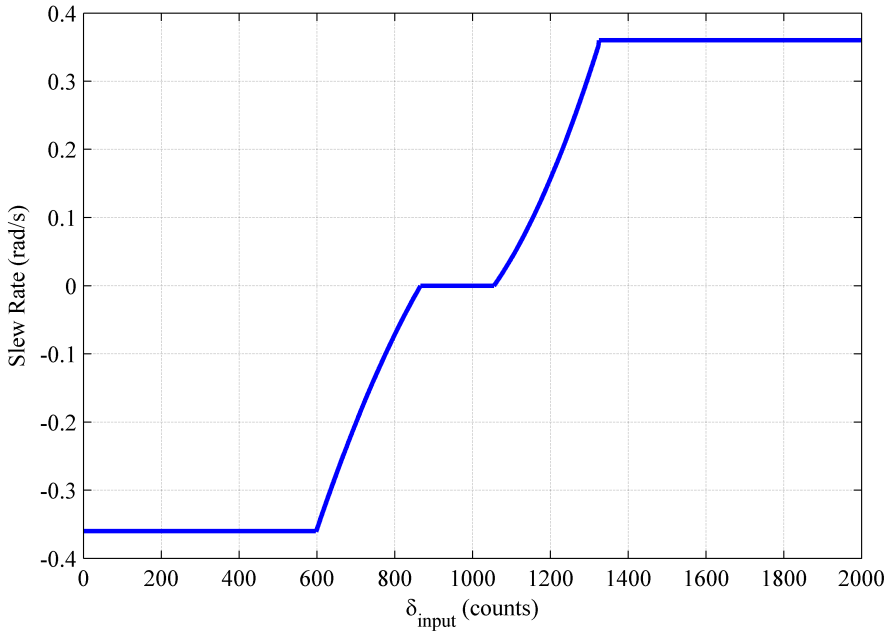

Figure 2.1: Steady State Slew Rate vs. Input Command

Table 2.1: Steady-State Slew Rate vs. Input Command Fits

Input Command (δ_{input})	Steady State Slew Rate ($\dot{\delta}$ (rad/s))
$\delta_{input} < 598$	$\dot{\delta} = -0.36$
$598 \leq \delta_{input} < 866$	$\dot{\delta} = -0.000001295\ \delta_{input}^2 + 0.00324\ \delta_{input} - 1.835$
$866 \leq \delta_{input} < 1055$	$\dot{\delta} = 0$
$1055 \leq \delta_{input} < 1325$	$\dot{\delta} = 0.000001859\ \delta_{input}^2 - 0.003111\ \delta_{input} + 1.213$
$\delta_{input} \geq 1325$	$\dot{\delta} = 0.36$

To counter the deadband and nonlinearities, an inverse lookup table was created by [Gartley, 2005] so that the input to output characteristics of the steering actuator are linear with the exception of saturation. The lookup table functions are listed in Table 2.2. Using the look-up table, the controller specifies a desired

Table 2.2: Inverse Mapping of Steady-State Slew Rate to Input Command

Intermediate Input Cmd ($\hat{\delta}_{input}$)	Input Command (δ_{input})
$\hat{\delta}_{input} < -0.36$	$\delta_{input} = 598$
$-0.36 \geq \hat{\delta}_{input} < 0$	$\delta_{input} = 518.7\ \hat{\delta}^2_{input} + 920.2\ \hat{\delta}_{input} + 864.4$
$0 \geq \hat{\delta}_{input} < 0.36$	$\delta_{input} = -887.9\ \hat{\delta}^2_{input} + 1045\ \hat{\delta}_{input} + 1059$
$\hat{\delta}_{input} \geq 0.36$	$\delta_{input} = 1325$

slew rate ($\hat{\delta}_{input}$) for the steering actuator and the proper count value is sent across the CAN. This makes the DC gain of the effective actuator input to steering slew rate transfer function equal to unity.

The entire steering actuator model from input to steering angle is represented by the schematic in Figure 2.2. The steering actuator controller commands a desired slew rate ($\hat{\delta}_{input}$) which is converted to the steering actuator input (δ_{input}) by inverting the nonlinearities. Next, the signal δ_{input} goes through the nonlinearities and model, and the slew rate ($\dot{\delta}$) gets integrated into the steering angle (δ).

Figure 2.2: Steering Actuator Model

Through system identification experiments conducted by [Gartley, 2005], the parameters seen in Table 2.3 were identified. The identified model is second order with no zeros as represented in Equation (2.1).

$$G_{P\delta} = \frac{\dot{\delta}(s)}{\hat{\delta}_{input}(s)} = \frac{\omega_n^2}{s^2 + 2\zeta\omega_n \cdot s + \omega_n^2} \tag{2.1}$$

Table 2.3: Steering Actuator Model Parameters

Parameter	Value
ω_n	28.425 rad/s
ζ	0.633
δ_{max}	32 deg
$\dot{\delta}_{max}$	20.6 deg/s

2.2.2 Dynamic Yaw Model

Previous studies have been done on modeling the effects of lateral hitch forces on yaw rate dynamics. A model has been proposed in which the farm implement is modeled as a third axle behind the tractor [O'Conner, 1997]. Another study has been conducted that has shown its validity for implements attached to the three-point hitch through experimentation [Pearson and Bevly, 2005]. Studies have also created implement models using soil mechanics that predict the longitudinal and vertical forces, but these studies lack the ability to predict the lateral forces needed to turn the implement [R. Berntsen and Aasen, 2006],
[Godwin and O'Dogherty, 2007], [Rosa and Wulfsohn, 1999],
[Sahu and Raheman, 2006]. Therefore, this research uses the model in which the implement is modeled as a tire to predict the effects of the implement on yaw dynamics.

The bicycle model of a vehicle lumps the inner and outer wheels of each axle into a single wheel. Therefore, the model inherently neglects weight transfer between the inner and outer wheels. A schematic of the tractor modeled as a

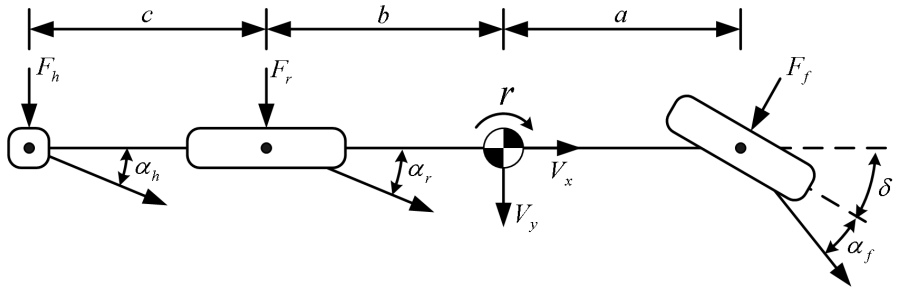

Figure 2.3: Bicycle Model with Augmented Hitch Force

bicycle is shown in Figure 2.3. Notice that the hitch force is modeled as an extra axle behind the rear axle. The lateral tire force at each axle (F_f, F_r, F_h) is a function of the slip angles $(\alpha_f, \alpha_r, \alpha_h)$ at each axle [Gillespie, 1992]. The slip angle is defined as the angle between the velocity vector and the heading of each axle. The linearized bicycle model assumes the steering and slip angles are small, and the lateral tire force is proportional to the slip angles at the respective axle. The proportionality constant is called the cornering stiffness and is denoted by $C_{\alpha f}, C_{\alpha r}, C_{\alpha h}$. The cornering stiffness is a function of normal force on the tire, but the normal force in this thesis is assumed to be constant. The hitch cornering stiffness ,$C_{\alpha h}$, is the parameter that changes with different implements. In reality, the lateral tire force reaches a point of saturation, but it will be assumed that the tires on the tractor stay in the linear region. The lateral tire force equations are represented by Equation (2.2).

$$
\begin{aligned}
F_f &= -C_{\alpha_f}\alpha_f \\
F_r &= -C_{\alpha_r}\alpha_r \\
F_h &= -C_{\alpha_h}\alpha_h
\end{aligned}
\tag{2.2}
$$

The lengths from the center of gravity to the front and rear axle are a and b, and the length from the rear axle to the hitch is c. The variables V_y and V_x are the lateral and longitudinal velocities at the center of gravity, δ is the steering angle of the front axle, and r is the yaw rate of the tractor. Using Newton's equations, the lateral forces and moments about the center of gravity are represented by Equation (2.3).

$$
\begin{aligned}
\textstyle\sum F_y &= m \cdot a_y = F_f \cos\delta + F_r + F_h \\
\textstyle\sum M_{CG} &= I_{zz}\dot{r} = a \cdot F_f \cos\delta - b \cdot F_r - (b+c) \cdot F_h
\end{aligned}
\tag{2.3}
$$

By assuming that the tractor is a rigid body, a kinematic relationship between velocity, yaw rate, steering angle, and slip angles can be formed. These relationships are shown in Equation (2.4).

$$\begin{aligned}
\alpha_f &= \tan^{-1}\left(\frac{V_y + r \cdot a}{V_x}\right) - \delta \\
\alpha_r &= \tan^{-1}\left(\frac{V_y - r \cdot b}{V_x}\right) \\
\alpha_h &= \tan^{-1}\left(\frac{V_y - r \cdot (b+c)}{V_x}\right)
\end{aligned} \tag{2.4}$$

The following equations can be combined to form a transfer function from steering angle to yaw rate. By linearizing assuming small slip and steering angles, the linear model shown in Equation (2.5) can be formed.

$$G_{Pr} = \frac{r(s)}{\delta(s)} = \frac{n_1 \cdot s + n_0}{d_2 \cdot s^2 + d_1 \cdot s + d_0} \tag{2.5}$$

Where:

$$\begin{aligned}
n_0 &= \frac{C_{\alpha f} C_1 + a C_{\alpha f} C_2}{m V_x} \\
n_1 &= a C_{\alpha f} \\
d_0 &= \frac{C_2 C_3 - C_1^2}{m V_x^2} + C_1 \\
d_1 &= \frac{C_2 I_{zz}}{m V_x} + \frac{C_3}{V_x} \\
d_2 &= I_{zz}
\end{aligned} \tag{2.6}$$

And:

$$
\begin{aligned}
C_1 &= ((b+c)\cdot C_{\alpha h} + b\cdot C_{\alpha r} - a\cdot C_{\alpha f}) \\
C_2 &= (C_{\alpha h} + C_{\alpha r} + C_{\alpha f}) \\
C_3 &= ((b+c)^2 C_{\alpha h} + b^2 C_{\alpha r} + a^2 C_{\alpha f})
\end{aligned}
\tag{2.7}
$$

The yaw model parameters of the tractor are shown in Table 2.4.

Table 2.4: Yaw Rate Model Parameters

Parameter	Value
a	1.00 m
b	2.00 m
c	2.19 m
I_{zz}	18500 kg $\cdot$ m^2
m	11340 kg
$C_{\alpha f}$	2400 N/deg
$C_{\alpha r}$	5000 N/deg
$C_{\alpha h}$	$0 - 4000$ N/deg
V_x	2 m/s

In this research, the yaw dynamics with respect to the cornering stiffness of the hitch is of primary interest. This is due to the face that once it is known how the lateral hitch force affects the yaw rate response, an adaptive controller can be designed to compensate for this variation. It has been shown empirically that $C_{\alpha h}$ can range from 0 N/deg with no implement to 4000 N/deg for a heavy implement [Pearson, 2007]. To investigate the differences in dynamic behavior caused by varying lateral hitch forces, a step input simulation was completed using MATLAB. The results of the simulation are shown in Figure 2.4. Notice that all

of the runs settle between 0.4 and 0.6 seconds, but the steady-state value varies significantly.

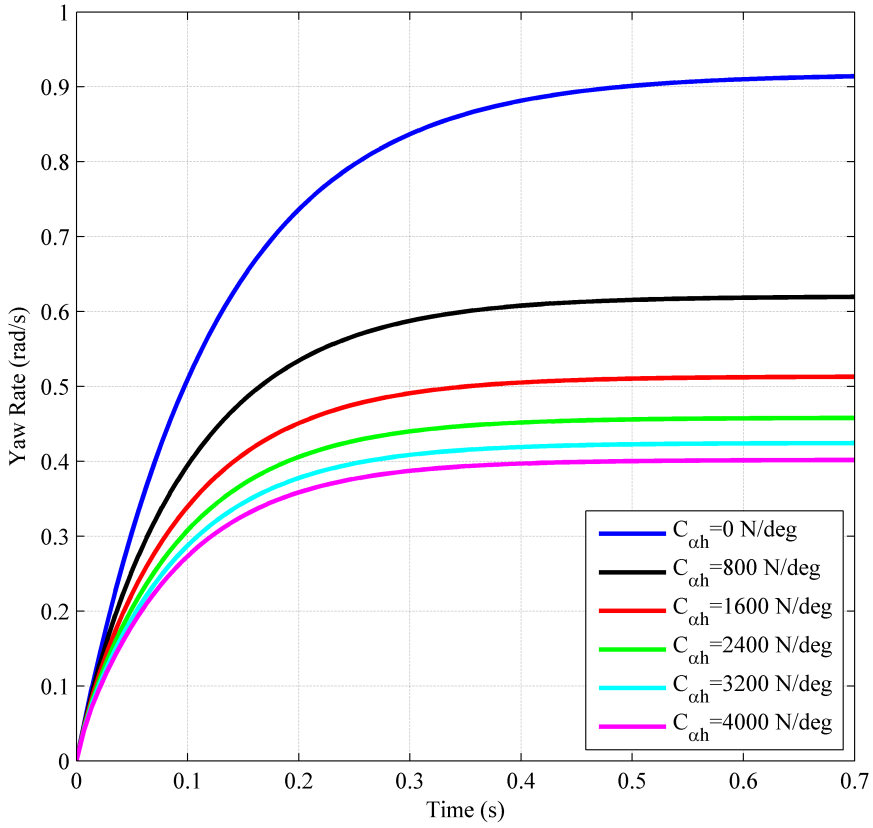

Figure 2.4: Step Response of Yaw Model with Varying $C_{\alpha h}$

A plot is shown in Figure 2.5 of the DC gain of the yaw rate transfer function verses $C_{\alpha h}$. It can be seen by looking at the black dotted line that $C_{\alpha h} = 600$ N/deg is the value of $C_{\alpha h}$ that results in the median DC gain value. This will be defined as the nominal value for the DC gain. Later in this chapter, this value of $C_{\alpha h}$ will be used to nominally tune the yaw rate controller.

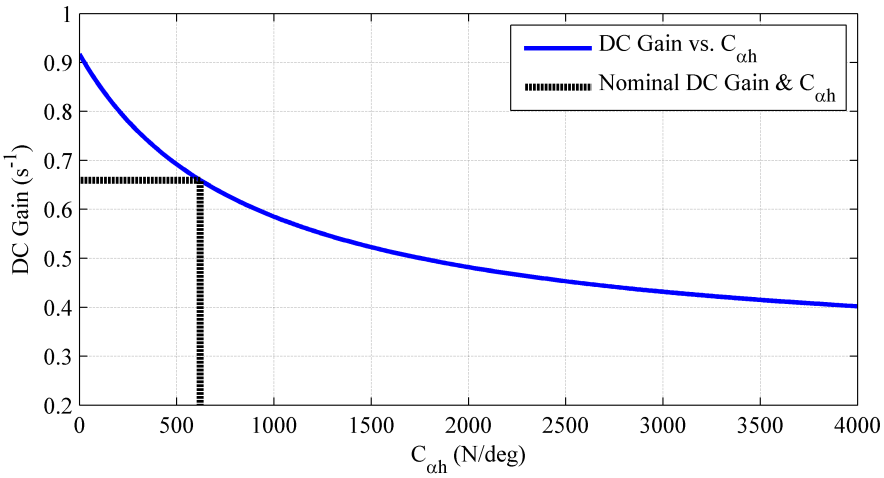

Figure 2.5: DC Gain of Yaw Model vs. $C_{\alpha h}$

It can also be observed in Figure 2.6 that the effect of $C_{\alpha h}$ on the primary pole is very small. Recall in Figure 2.4 this change in the dynamics was barely noticeable in the previously shown step response plots.

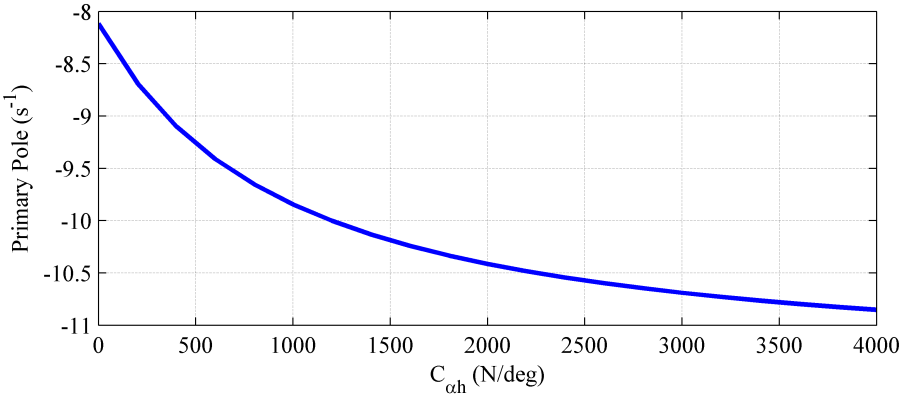

Figure 2.6: Primary Pole of Yaw Model vs. $C_{\alpha h}$

It is shown in Figure 2.7 that the secondary pole changes more than three-fold over the range of $C_{\alpha h}$. However, since the secondary pole is 5-15 times faster that

the primary pole, the effect of secondary pole on the yaw rate response is negligible. From the previous plots, it can be concluded that the DC gain of the steering angle to yaw rate transfer function is the parameter that changes the response the most with respect to variable hitch loading. Therefore, the transient dynamics can reasonably be assumed to be constant with respect to $C_{\alpha h}$. Because of these properties, an adaptive controller will be developed in this thesis to compensate only for the change in DC gain of the steering angle to yaw rate transfer function.

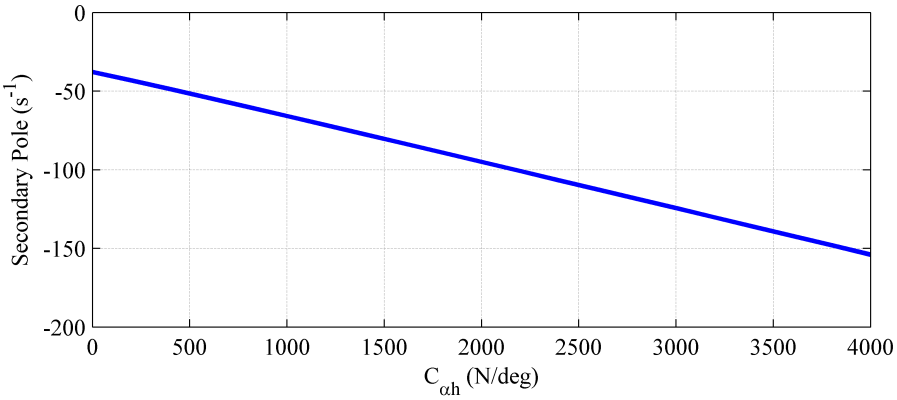

Figure 2.7: Secondary Pole of Yaw Model vs. $C_{\alpha h}$

2.2.3 Lateral Position Model

A kinematic relationship between yaw rate and lateral position is used as the lateral position plant model. A diagram is shown in Figure 2.8 that describes the relationship. Lateral position (y) can be described by Equation (2.8) where β is the side slip angle at the center of gravity, ν is the course angle of the velocity

vector with respect to the desired longitudinal direction, and V is the magnitude of velocity.

$$\begin{aligned} \dot{y} &= V \sin(\nu) \\ \dot{\nu} &= r + \dot{\beta} \end{aligned} \tag{2.8}$$

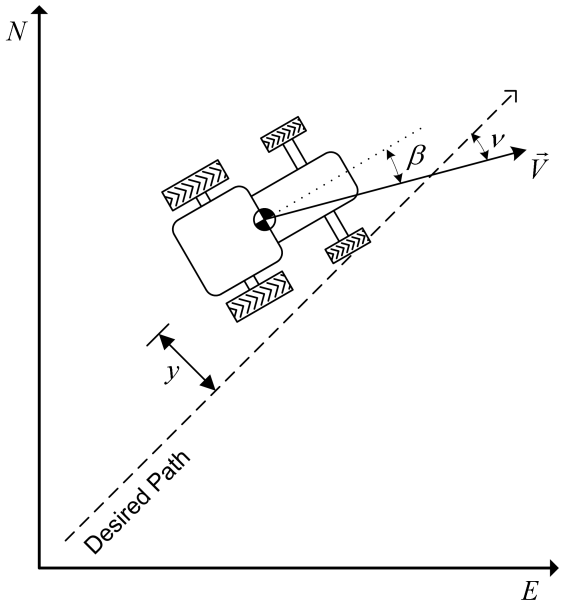

Figure 2.8: Lateral Position Schematic

Lateral velocity is the total velocity times the sine of the course angle, and the course angle is defined as the integrated yaw rate plus side slip angle. Neglecting side slip and linearizing assuming small angles yields the transfer function from yaw rate to lateral position shown in Equation (2.9).

$$G_{Py} = \frac{y(s)}{r(s)} = \frac{V}{s^2} \tag{2.9}$$

2.3 Control Structure and Design

2.3.1 Control Structure

In order to regulate the lateral position of the farm tractor, a controller system must be designed to regulate the three subsystems described in the previous sections. A cascaded controller is advantageous because the three subsystems can be individually controlled using classical control techniques. Also, a cascaded controller allows more than one measurement to be fed back to produce a more accurate response [Levine, 1996]. A diagram of the cascaded controller network is shown in Figure 2.9.

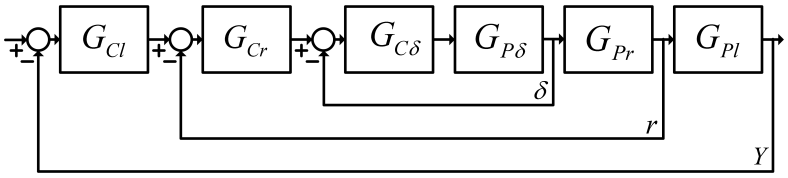

Figure 2.9: Cascaded Controller Block Diagram

The boxes labeled $G_{P\delta}$, G_{Pr}, and G_{Pl} are the steering actuator, yaw rate, and lateral position plants, respectively. The boxes labeled $G_{C\delta}$, G_{Cr}, and G_{Cl} are the steering actuator, yaw rate, and lateral position controllers. The three measurements being fed back are the steering angle (δ), yaw rate (r), and lateral position (y). Note that all of the analysis in the following sections is performed at $V = 2$ m/s.

2.3.2 Steering Actuator Controller Design

As was discussed in a Section 2.2.1, the steering actuator dynamics are second order with an integrator. Because the steering actuator has a pure integrator, the system is type one. This means that there is zero steady state error in a step response [Dorf and Bishop, 2005]. The system type combined with the system being well damped allows a proportional control law to be used. The control law is described by Equation (2.10) with the parameters being described in Equation (2.11).

$$G_{C\delta} = \frac{\delta_{input}(s)}{\delta_{err}(s)} = k_{p\delta} \tag{2.10}$$

$$k_{p\delta} = 3.84 \tag{2.11}$$

Equation (2.12) shows the closed-loop transfer function of the steering actuator dynamics.

$$G_{\delta_{CL}} = \frac{\delta(s)}{\delta_{des}(s)} = \frac{k_{p\delta}\omega_n^2}{s^3 + 2\zeta\omega_n \cdot s^2 + \omega_n^2 \cdot s + k_{p\delta}\omega_n^2} \tag{2.12}$$

To analyze the closed loop performance and stability, a root locus analysis was performed. The root locus plot can be seen in Figure 2.10. The closed-loop poles are denoted in the figure by the triangles. Tuning of $k_{p\delta}$ was performed so that the steering actuator would have the highest possible bandwidth without

oscillation. The location, natural frequency, and damping ratios for each of the three closed-loop poles are listed in Table 2.5.

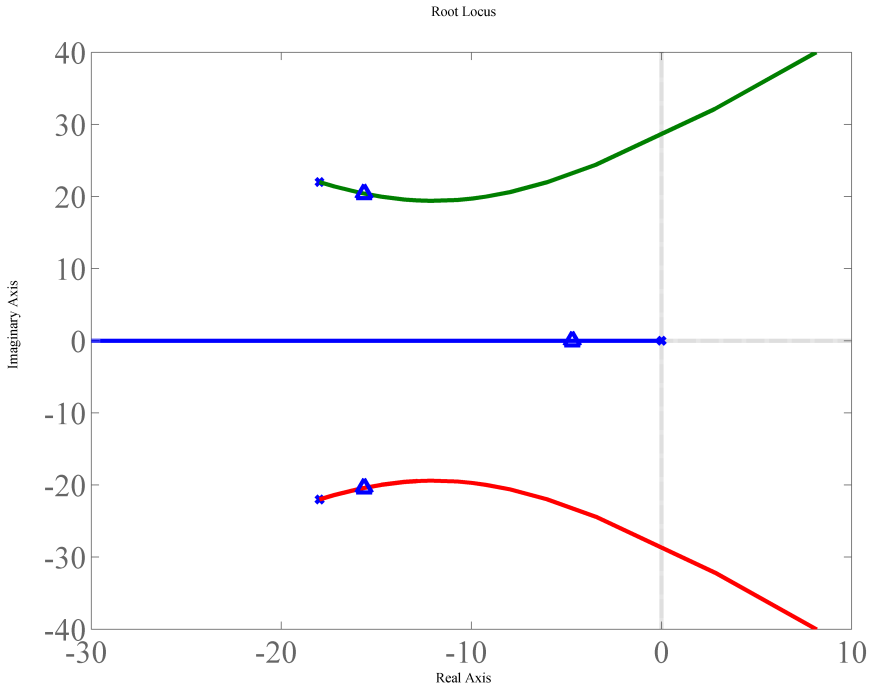

Figure 2.10: Steering Actuator Root Locus and Closed-Loop Pole-Zero Locations for $k_{p\delta} = 3.84$

Table 2.5: Steering Actuator Controller Closed-Loop Pole Properties

Pole Location	Damping Ratio	Frequency (rad/s)
$-15.6465 + 20.4036i$	0.609	25.7123
$-15.6465 - 20.4036i$	0.609	25.7123
-4.6930	1	4.6930

2.3.3 Yaw Rate Controller Design

The yaw rate plant has two poles that are over-damped. In steady state, the desired yaw rate will be approximately equal to zero because the tractor will be tracking a straight line. Because of these two properties, a proportional control law will also be used to regulate the yaw rate. The equation of the control law is shown in Equation (2.13), and the controller coefficient values are shown in Equation (2.14).

$$G_{Cr} = \frac{\delta_{des_{fb}}(s)}{r_{err}(s)} = k_{pr} \tag{2.13}$$

$$k_{pr} = 0.30 \tag{2.14}$$

Equation (2.15) shows the closed-loop transfer function of the yaw rate dynamics.

$$G_{r_{CL}} = \frac{r(s)}{r_{des}(s)} = \frac{k_{pr} G_{\delta_{CL}} (n_1 s + n_0)}{d_2 s^2 + (d_1 + n_1 k_{pr} G_{\delta_{CL}}) s + d_0 + n_0 k_{pr} G_{\delta_{CL}}} \tag{2.15}$$

The term $G_{\delta_{CL}}$ is the closed loop dynamics of the steering actuator.

In order to analyze the dynamics and stability of the closed-loop behavior, a root locus analysis is again used. While designing the yaw rate controller, the inner-loop steering actuator dynamics are included in the analysis because the bandwidths of the two systems are similar. The root locus plot is shown in Figure 2.11, where the closed loop poles are noted by triangles. The five closed-loop pole locations, damping ratios, and frequencies are shown in Table 2.6. The slower poles dominate the response.

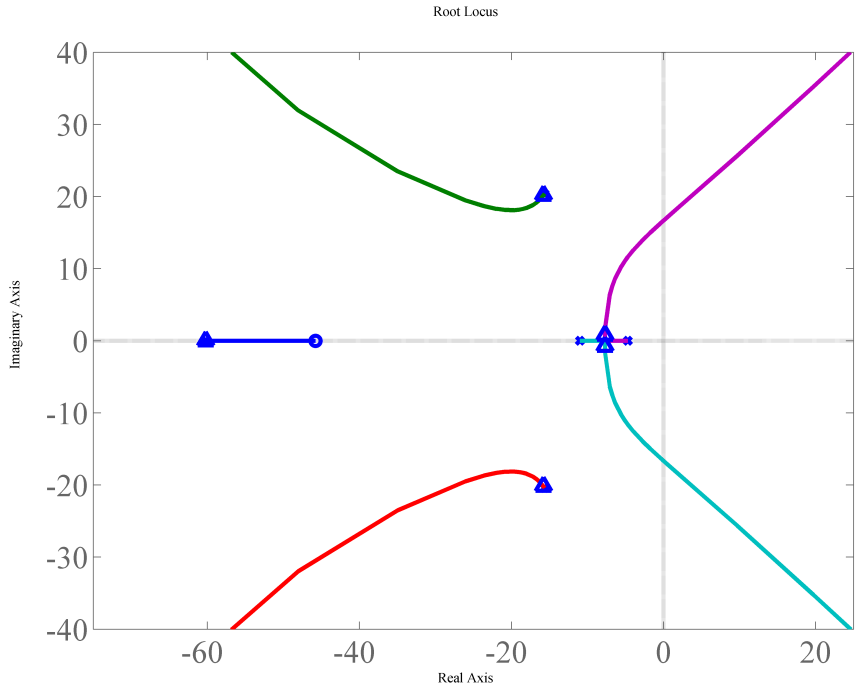

Figure 2.11: Yaw Rate Root Locus and Closed-Loop Pole-Zero Locations for $k_{pr} = 0.30$

Table 2.6: Yaw Rate Controller Closed-Loop Pole Properties

Pole Location	Damping Ratio	Frequency (rad/s)
$-7.7062 + 0.7552i$	0.995	7.7431
$-7.7062 - 0.7552i$	0.995	7.7431
$-15.7899 + 20.1817i$	0.616	25.6246
$-15.7899 - 20.1817i$	0.616	25.6246
-60.2030	1	60.2030

2.3.4 Lateral Position Controller Design

The lateral position controller is chosen to be a standard proportional-integral-derivative (PID) controller. Since the two open-loop poles of the lateral position plant are at the origin, there needs to be some damping that will be supplied by the derivative term of the controller. Also, the integral term will offset any steady-state error cause by calibration errors or unlevel terrain. The equation of the controller is shown in Equation (2.16), and the coefficients are described in Table 2.7.

$$G_{Cy} = \frac{r_{des}(s)}{y_{err}(s)} = k_{py}(1 + \frac{k_{iy}}{s} + k_{dy} \cdot s) \tag{2.16}$$

The inner-loop yaw rate dynamics can be neglected since they are many times faster that the lateral position dynamics. Only the DC gain of the inner-loop transfer function will have to be included. Equation (2.17) describes the closed-loop lateral position dynamics neglecting the yaw rate dynamics.

$$G_{y_{CL}} = \frac{y(s)}{y_{des}(s)} = \frac{V \cdot DC_{yaw}(k_{py} \cdot s + k_{dy} \cdot s^2 + k_{iy})}{V \cdot DC_{yaw}(k_{py} \cdot s + k_{dy} \cdot s^2 + k_{iy}) + s^3} \tag{2.17}$$

As can be seen, the lateral position dynamics are a function of velocity and the DC gain of the closed-loop yaw rate transfer function. Since it is desired that the tractor's lateral position response be the same for all implements, it is critical that DC_{yaw} remain nearly constant. This is the reason the yaw rate controller will be adapted. The value of DC_{yaw} is to be determined in a later chapter, so the controller values shown in Table 2.7 are represented as a function of this variable. By adjusting the proportional controller coefficient by the inverse of DC_{yaw}, the reference yaw rate is scaled so that the DC gain of the yaw rate response is effectively unity.

Table 2.7: Lateral Position Controller Coefficients

Coefficient	Value
k_{py}	$0.10/DC_{yaw}$
k_{pd}	2.50
k_{pi}	0.01

Root locus is again used to analyze the controller as shown in Figure 2.12. The closed-loop poles are again marked by the triangles. The closed-loop pole locations, damping ratio, and frequencies are listed in Table 2.8.

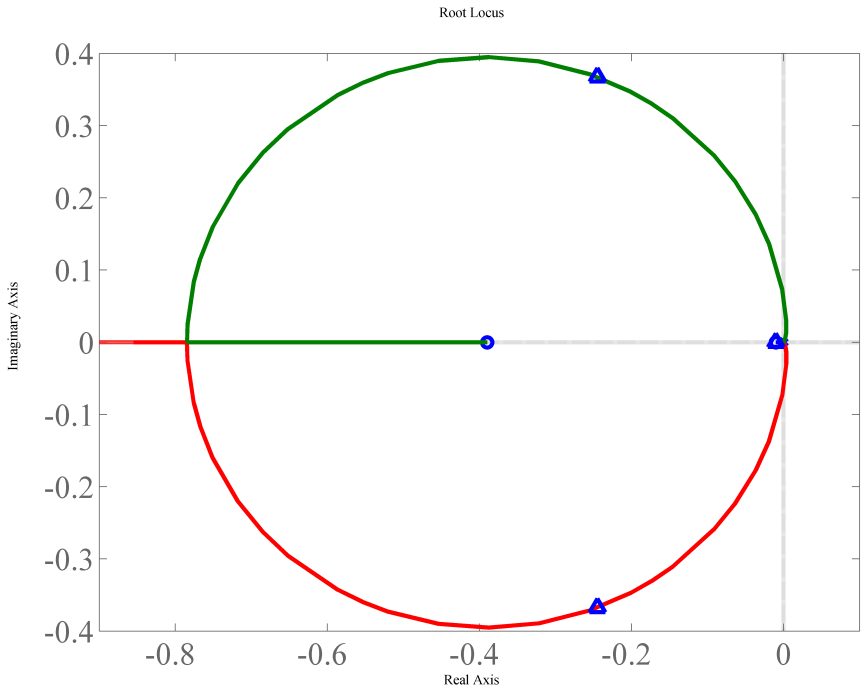

Figure 2.12: Lateral Position Root Locus and Closed-Loop Pole-Zero Locations

Table 2.8: Lateral Position Controller Closed-Loop Pole Properties

Pole Location	Damping Ratio	Frequency (rad/s)
$-0.2449 + 0.3674i$	0.555	0.4415
$-0.2449 - 0.3672i$	0.555	0.4415
-0.0103	1	0.0103

2.4 Summary and Conclusions

This chapter has discussed the system models and control architecture that affect the lateral position control of the John Deere 8420 farm tractor. The steering actuator model was presented including a lookup table that makes the input to

output characteristics linear. A dynamic yaw rate model was discussed that allows the lateral hitch force to be time varying. The change in the yaw rate response with respect to hitch loading was shown to be dominated by the DC gain of the steering angle to yaw rate transfer function. Next, a kinematic model of the lateral position plant was presented. Finally, the control architecture including design of gains was presented using root locus analysis.

Chapter 3

Adaptive Control by Compensating Yaw Rate Loop Gain

3.1 Introduction

This chapter presents a model reference adaptive control (MRAC) algorithm used to compensate for the change in the DC gain of the steering angle to yaw rate transfer function due to changing hitch forces. The algorithm accomplishes this by adapting the loop gain of the closed-loop yaw rate control system. Different adaptive control methods exist, and a brief review is completed that describes different methods considered for this research and why a MRAC was chosen. The adaptation system is presented with a series of block diagrams, and the adaptation algorithm is derived. A preliminary simulation is presented that shows the performance of the MRAC system while neglecting the inner-loop steering actuator properties. The MRAC system is modified to include the steering actuator properties, and more simulation results are presented that demonstrate the improved performance of the adaptation system. Finally, experimental results are presented that prove the algorithm can be implemented on a real system. The performance of the algorithm is discussed including shortcomings and benefits.

3.2 Adaptive Control Techniques

Adaptive control techniques are advantageous because controllers can be adjusted to match changes in the plant they are trying to regulate. There are several techniques in the literature, and a list of methods that were considered in this research includes indirect self-tuning, direct self-tuning, gain scheduling, and MRAC. A brief discussion of each will be presented, and reasons will be given to justify the decision to implement a MRAC system. A more in depth description of each method can be found in [Astrom and Wittenmark, 1995].

Direct and indirect self-tuning regulators have been around for decades and are similar. The first paper presenting the self tuning idea came out in the middle of the twentieth century [Kalman, 1958]. Indirect self-tuning regulators rely on estimation techniques such as recursive least squares to estimate plant parameters. Once the plant parameters are known, methods such as pole placement are used to design the controller. Direct self-tuning regulators, on the other hand, estimate the controller parameters directly with no intermediate estimation of model parameters. This is accomplished by a reparameterization of the controller design equations into the system model. The goal of this research is to design a direct method of adapting the yaw rate controller; therefore, the indirect self-tuning regulator will not be investigated any further. A direct method is desired so that there are no complications associated with pole placement. A direct self-tuning would work for a general yaw rate plant, but the steering actuator has saturations that

cannot be accounted for using a linear estimation technique. Therefore, a direct self-tuning regulator cannot ideally be implemented on the farm tractor.

Gain scheduling is advantageous when it is known how an auxiliary system parameter affects the system performance. In the case of the farm tractor, the type of implement would be the auxiliary variable. A series of off-line system identification experiments could be completed to document how the implement affects the yaw dynamics, and a schedule of controller gains could be formed to compensate for different implements. For this solution to be viable, however, every implement the farmer uses would have to be identified. While this is doable, it does not take into account varying soil conditions and depth of the implement. Because soil moisture and soil type plays an important role in implement-soil mechanics, neglecting this factor would not be a good solution.

A MRAC system compares the outputs of a model and plant, and through an adaptation mechanism adjusts the controller so that the difference in the outputs go to zero. There are two methods to produce the adaptation algorithm: gradient techniques and stability techniques. The gradient technique uses a cost function of the error between model and plant. The adaptation law is formed by moving the controller parameters in the direction of the negative gradient of the cost function with respect to the controller parameters. This method is appealing because the algorithm is straight forward to derive. The problem is that general stability has not been proven for this method. Stability of a time invariant plant using the gradient technique has been proven, but this cannot be applied to the tractor

system since the yaw rate plant is time varying [Mareels, 1989]. The stability techniques generally use a Lyapunov function that consists of the states of the system and mismatch functions. The mismatch functions are equal to zero if the plant perfectly matches the model. The adaptation algorithm is formed by making the time rate of change of the Lyapunov function negative semi-definite. The problem with applying this method to the farm tractor is that the mismatch functions cannot be formed due to approximations that will be described in later sections. For these reasons, the gradient technique is used in this thesis to adapt the yaw rate controller. Issues with proving stability will be resolved with experimental testing. This method is advantageous because a good model is known that predicts how the yaw rate dynamics change with hitch loading. Therefore, the closed-loop yaw rate model will be tuned to a desired configuration, and the plant yaw rate controller will be adjusted using a gradient MRAC system so that the plant output matches the model.

3.3 MRAC-LGA Algorithm

This section presents the layout and update law of the MRAC loop gain adaptation algorithm. A schematic is shown that describes all of the different components that are required to implement a MRAC system. The value of the adaptation gain to drive the plant dynamics to match the model dynamics is calculated. Finally, the update law is derived representing the time rate of change

of the adaptation gain with respect to the reference yaw rate, plant output, and model output.

3.3.1 Adaptation System Architecture

A MRAC system consists of a plant, model, controller, and adaptation mechanism. The goal of the system is to adjust the controller so that the output of the plant matches the output of the model with respect to the same reference input. Figure 3.1 shows the layout of the system.

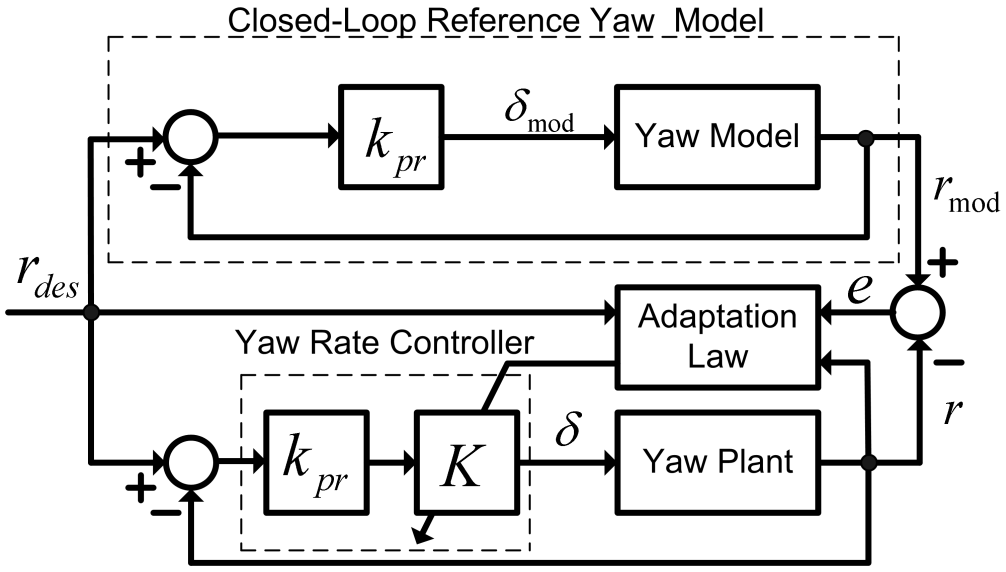

Figure 3.1: MRAC System Block Diagram

As can be seen in the figure, the desired yaw rate is sent through the model dynamics and plant dynamics. The model dynamics is the area encircled by a dashed line and labeled "Closed-Loop Reference Yaw Model." The model dynamics consists of the yaw rate model, a fixed-gain yaw rate controller, and a feed-back

loop. The area encircled by a dashed line and labeled "Yaw Rate Controller" is the transfer function G_{Cr} described in Chapter 2. The yaw rate controller consists of a fixed proportional gain multiplied by an adaptation gain K. The two outputs are compared, and the difference (e) is used as the input in the adaptation mechanism along with the plant output and reference yaw rate.

3.3.2 LGA Algorithm Derivation

The purpose of the adaptation law is to make the closed-loop yaw dynamics constant while in the presence of the varying hitch cornering stiffness. The desired yaw dynamics are represented by the closed-loop reference yaw model, and the adaptation law is used to match the plant output to the output of the reference model. This is accomplished when the model and plant are equal. As was discussed in Chapter 2, the DC gain of the steering angle to yaw rate transfer function is the parameter that dominates the change in yaw dynamics with respect to hitch loading. Therefore, the proportional control law will be adjusted to offset any changes in the DC gain of the steering angle to yaw rate transfer function.

Equation (3.1) represents the closed-loop plant and closed-loop reference model.

$$G_{r_{CL}} = \frac{K k_{pr} k_{DC_{trac}} G}{1 + K k_{pr} k_{DC_{trac}} G} = \frac{k_{pr} k_{DC_{mod}} G}{1 + k_{pr} k_{DC_{mod}} G} \tag{3.1}$$

The left transfer function represents the actual closed-loop yaw dynamics, and the right transfer function represents the reference model's closed-loop dynamics. As can be seen, the yaw rate plant, G_{Pr}, has been replaced by $k_{DC_{trac}}$ times G.

The variable $k_{DC_{trac}}$ is the DC gain of the actual yaw rate transfer function, and G represents the yaw rate transfer function dynamics. The variable $k_{DC_{mod}}$ represents the DC gain of the reference model yaw rate transfer function. It is assumed that the dynamics, G, of the steering angle to yaw rate transfer function are constant and the only variable that changes with hitch loading is $k_{DC_{trac}}$. For this equation to be equal on both sides, K times $k_{DC_{trac}}$ must be equal to $k_{DC_{mod}}$. Therefore, Equation (3.2) represents the value that the adaptation gain must be in order to keep the closed-loop yaw dynamics equal for all hitch loadings.

$$K_{match} = \frac{k_{DC_{mod}}}{k_{DC_{trac}}} \tag{3.2}$$

As was previously discussed, the gradient MRAC approach will be used to derive the adaptation law. The MIT Rule is an approach to gradient based MRAC [Whitaker and Kezer, 1958]. In order to derive the adaptation law, a cost function of the error between the model and plant must be formed. The cost function and error definition for the tractor are shown in Equation (3.3) where r is yaw rate.

$$\begin{aligned} e &= r_{mod} - r \\ J &= \tfrac{1}{2}e^2 \end{aligned} \tag{3.3}$$

The MIT Rule creates the adaptation law by moving the adaptation gain in the negative direction of the cost function gradient with respect to the adaptation gain as seen in Equation (3.4).

$$\frac{dK}{dt} = -\gamma \frac{\partial J}{\partial K} \tag{3.4}$$

The variable γ is called the adaptation algorithm gain, and it changes the speed that the algorithm converges. This parameter is field tuned so that the convergence rate is suitable and the algorithm has a smooth response. If the gain is too high, there may be convergence issues due to noise. By using the chain rule, Equation (3.4) can be reduced to Equation (3.5)

$$\frac{dK}{dt} = -\gamma e \frac{\partial e}{\partial K} \tag{3.5}$$

Since $e = r_{mod} - r$ and r_{mod} does not contain terms with K, the adaptation law can be represented by Equation (3.6).

$$\frac{dK}{dt} = \gamma e \frac{\partial r}{\partial K} \tag{3.6}$$

To apply the previous equation to the system, an equation must be formed to represent the yaw rate plant output (r). The closed-loop yaw rate transfer function of the plant is shown in Equation (3.7).

$$G_{r_{CL}} = \frac{r(s)}{r_{des}(s)} = \frac{K k_{pr} G_{Pr}}{1 + K k_{pr} G_{Pr}} \tag{3.7}$$

By taking the inverse Laplace transform, the plant output differential equation shown in Equation (3.8) can be derived.

$$r = \frac{1}{d_0 + k_{pr} K n_0}(k_{pr} K(n_1(\dot{r}_{des} - \dot{r}) + n_0 r_{des}) - d_1 \dot{r} - d_2 \ddot{r}) \tag{3.8}$$

The n_i and d_i coefficients come from Equation (2.5). By applying the formula shown in Equation (3.6), the adaptation law in Equation (3.9) is formed.

$$\begin{aligned} \frac{dK}{dt} &= \gamma\beta(n_1 d_0(\dot{r_{des}} - \dot{r}) + n_0(d_0 r_{des} + d_1 \dot{r} + d_2 \ddot{r})) \cdot e \\ \beta &= \frac{k_{pr}}{(d_0 + k_{pr} K n_0)^2} \end{aligned} \tag{3.9}$$

As can be seen in the previous equation, the adaptation law is a function of the unknown parameter $C_{\alpha h}$ since the n_i and d_i coefficients are a function of that variable. The unknown values can either be absorbed into the adaptation algorithm gain, γ, or approximated by using the nominal $C_{\alpha h}$ parameter from Chapter 2. Since this algorithms varies the loop gain of the yaw rate control system, the algorithm will be called the Loop Gain Adaptation (LGA) system.

3.4 Simulations of the LGA Algorithm

In this section, simulation results re presented that describe the adaptation algorithm's performance. Table 3.1 list the values of all parameters used in the simulations.

Table 3.1: Parameters Used in LGA Simulations

Parameter	Value
a	1.00 m
b	2.00 m
c	2.19 m
I_{zz}	18500 kg $\cdot$ m^2
m	11340 kg
$C_{\alpha f}$	2400 N/deg
$C_{\alpha r}$	5000 N/deg
$C_{\alpha h,mod}$	600 N/deg
$C_{\alpha h,trac}$	4000 N/deg
V_x	2 m/s
k_{pr}	0.30
$k_{p\delta}$	3.84
γ	200

3.4.1 Simulation Results with Initial LGA Algorithm

To test performance of the adaptation law, a MATLAB simulation was developed. A reference yaw rate signal was fed in to the system shown previously in Figure 3.1. The LGA is effectively estimating the DC gain of the yaw rate plant. In order for the estimate to converge, there has to be at least a constant, non-zero input [Astrom and Wittenmark, 1995]. To further insure convergence, a single frequency was used for the reference signal, and the adaptation parameter should reach K_{match} in a finite amount of time.

The yaw rate plant includes the steering actuator properties. To force the steering actuator to become saturated, a cosine function was used as the reference signal. The cosine signal creates a large initial yaw rate error so that the steering actuator experiences saturation. The yaw rate reference model uses the nominal

value of $C_{\alpha h} = 600$ N/deg and the yaw rate plant was simulated with $C_{\alpha h} = 4000$ N/deg. A nominal velocity of 2 m/s was used in all simulations.

The adaptation gain and yaw rate responses are shown in Figure 3.2. Note that there is significant overshoot in the adaptation gain response, and the adaptation gain never converges to the desired value. Because the adaptation gain is not at the right value, the yaw rate of the tractor does not match the reference model. The steering angle and steering angle rate responses are shown in Figure 3.3. It can be noted that the steering angle of the model reaches the set point instantly, and there is a lag in the response of the plant steering angle. This is because there are no steering actuator properties included into the reference model.

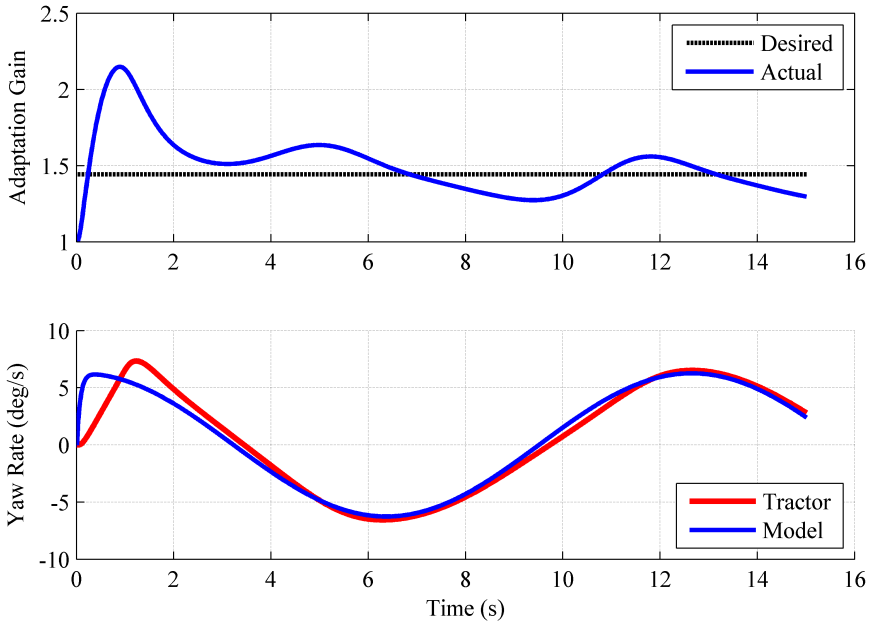

Figure 3.2: Simulated Adaptation Gain and Yaw Rate Response with Initial LGA Algorithm

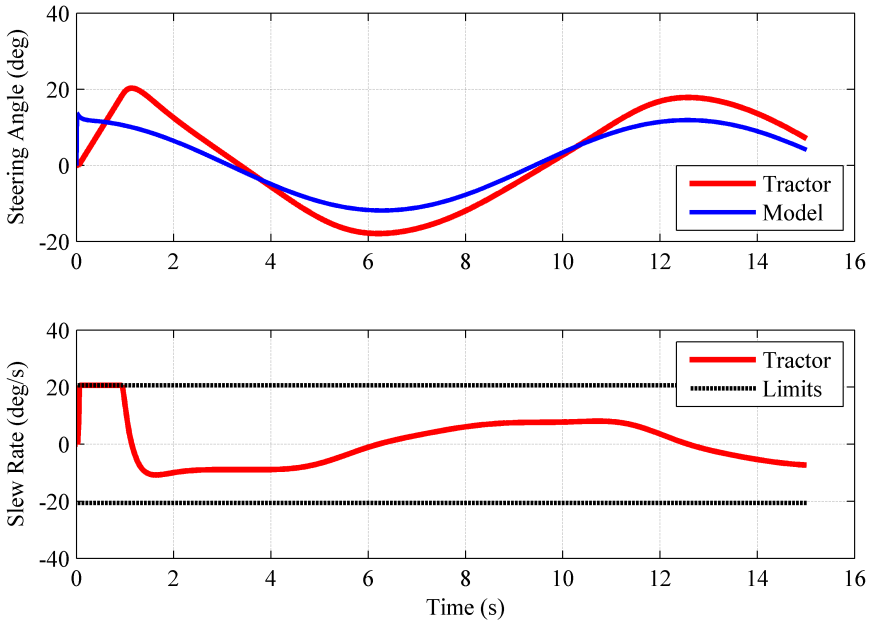

Figure 3.3: Simulated Steering Actuator Response with Initial LGA Algorithm

Additionally, a good bit of the lag in the steering angle response can be accounted to the steering angle rate of the plant becoming initially saturated as well as the dynamics associated with the actuator. Since there is instant steering angle into the yaw rate reference model, the adaptation gain becomes large to compensate for the difference in output between the reference model and plant. From this simulation, it can be determined that the adaptation mechanism will not function satisfactorily due to neglected actuator dynamics.

3.4.2 LGA Algorithm Modifications

In order to properly account for the steering actuator, the inner-loop steering actuator dynamics must be included into the algorithm. However, deriving a new

algorithm that takes the steering actuator into account results in a higher order solution. A higher order algorithm would require higher order derivatives of the outputs. This is not practical because high order derivatives of yaw rate are not measurable, and differentiation is too noisy.

However, if the gradient formed in Equation (3.9) could be used as an approximate solution, the inner-loop steering actuator dynamics can be included into the reference model while using the same algorithm derived by neglecting the steering actuator. This would allow the same order adaptation algorithm to be used as before, yet allowing the model to more closely depict the actual system. The new reference model block diagram is shown in Figure 3.4.

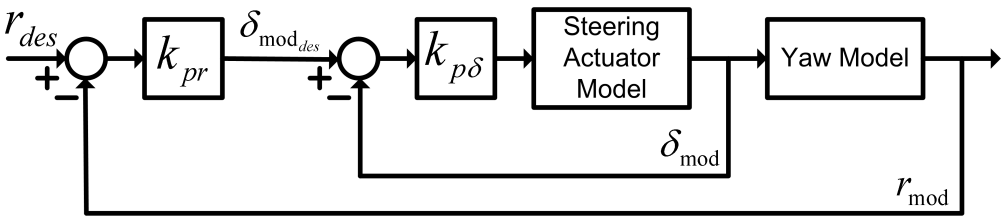

Figure 3.4: MRAC-LGA Closed-Loop Reference Model

The new adaptation and controller system is created by combining the systems shown in Figures 2.9, 3.1, and 3.4. A block diagram of this total system in shown in Figure 3.5. As can be seen, the lateral position controller commands a desired yaw rate based off of the lateral position error. The desired yaw rate is fed into the yaw rate plant, yaw rate model, and adaptation mechanism. Inside the closed-loop yaw rate plant and model are the steering actuator dynamics.

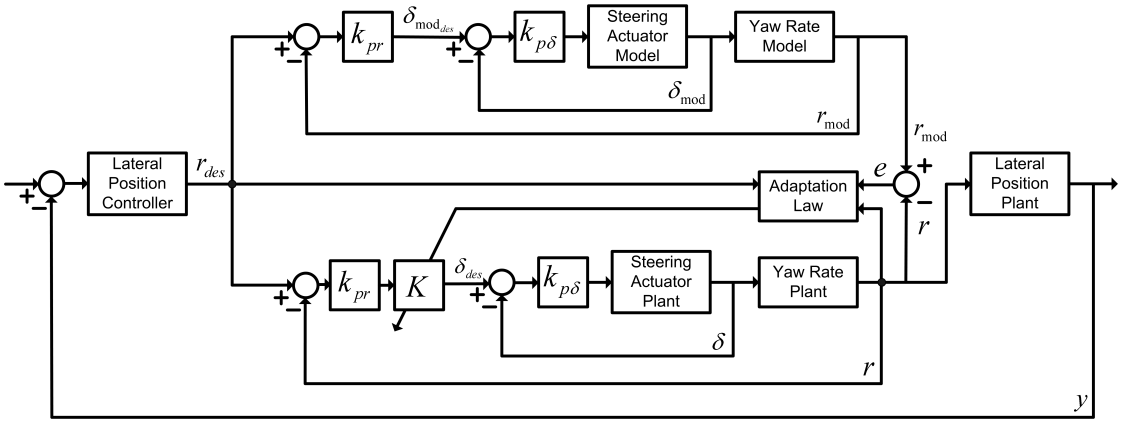

Figure 3.5: MRAC-LGA Total System Block Diagram

The steering actuator saturations are also put into the reference model. The steering angle and steering angle rate of the reference model are limited to the same values listed in Table 2.3. This adds another depth of fidelity to the model and will mitigate the overshoot seen previously in Figure 3.2. The model steering actuator will follow Equations (3.10) and (3.11).

$$\delta_{mod_{max}} = \delta_{max} \tag{3.10}$$

$$\dot{\delta}_{mod_{max}} = \dot{\delta}_{max} \tag{3.11}$$

During periods when the steering actuator is saturated, the gradient of the system shown in Equation (3.9) is not a good approximation for the system. This is due to the strong nonlinearities caused by the saturations. To account for this,

the adaptation gain K will be held constant during periods of saturations using the constraints provided in Equation (3.12).

$$\frac{dK}{dt} = \begin{cases} \frac{dK}{dt} & \text{for} \quad |\dot{\delta}_{meas}| < \dot{\delta}_{max} \quad |\delta_{meas}| < \delta_{max} \\ 0 & \text{for} \quad |\dot{\delta}_{meas}| \geq \dot{\delta}_{max} \quad |\delta_{meas}| \geq \delta_{max} \end{cases} \tag{3.12}$$

Although the system is not adapting when the steering actuator is saturated, the algorithm can be implemented on a system that experiences actuator saturations.

3.4.3 Simulation Results with Modified LGA Algorithm

To show that the approximated gradient algorithm works for the total system, another MATLAB simulation was created using the same reference signal as the simulation of the initial LGA algorithm. As was done in the previous simulation, the sensors were assumed to be noise and bias free. The hitch cornering stiffness for the reference model was again set to $C_{\alpha h} = 600$ N/deg and the yaw rate plant was simulated with $C_{\alpha h} = 4000$ N/deg. As was the case in the initial LGA simulation, the plant was modeled with the steering actuator dynamics and nonlinearities so that the simulated plant closely matches the actual tractor system. The major difference is that the reference model also had the steering actuator dynamics and nonlinearities.

The adaptation gain and yaw rate response from the simulation are shown in Figure 3.6. Notice that the large overshoot is mitigated as compared to Figure 3.2, and the yaw rate output from the plant converge to the same value when the

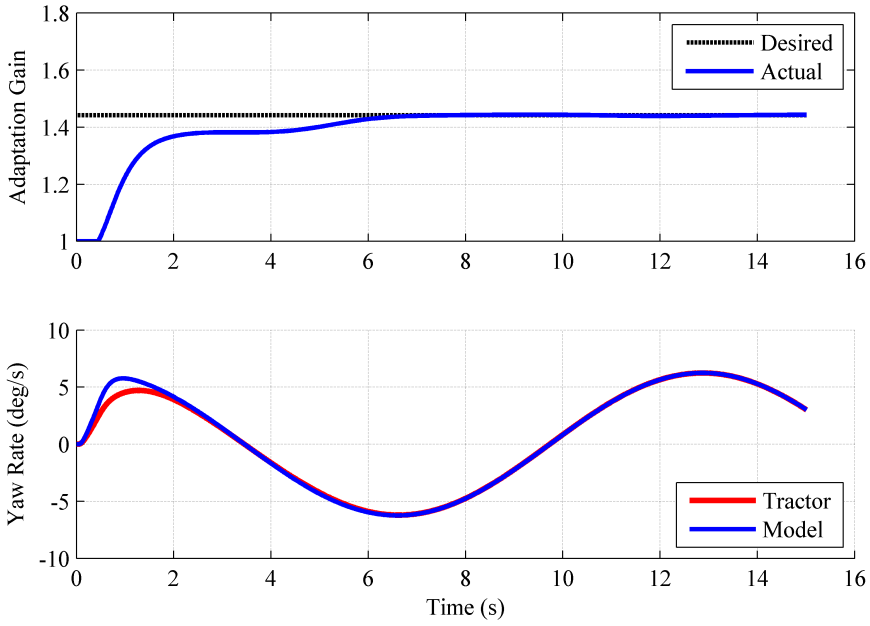

Figure 3.6: Simulated Adaptation Gain and Yaw Rate Response with Modified LGA Algorithm

adaptation gain reaches the desired value. This is the desired performance of the MRAC system. The steering actuator response can be seen in Figure 3.7.

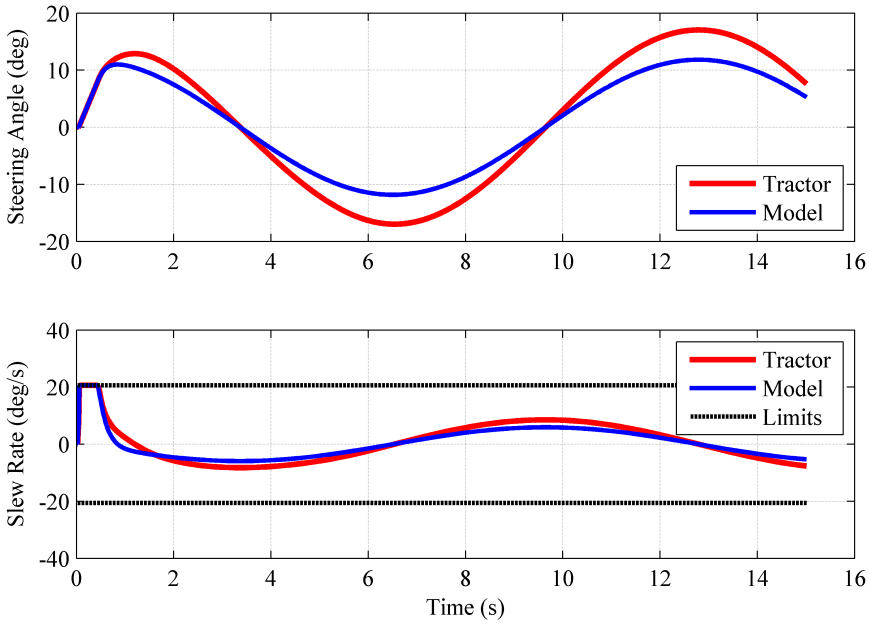

Figure 3.7: Simulated Steering Actuator Response with Modified LGA Algorithm

Observe in the steering angle response that the slew rate of the plant and reference model are initially saturated. This causes additional lag in the steering angle response on top of the dynamics. It can be seen in Figure 3.6 that the adaptation gain is held constant at a value of one during the slew rate saturation period. Also notice that there is more steering angle being applied to the plant than the model. This is because there is more steering angle needed to turn the bigger implement. This simulation shows that the modified LGA algorithm can be implemented on a system that has actuator saturations and non-negligible dynamics. Also, the simulation shows that the gradient calculated from the system with neglected steering actuator dynamics can be implemented on a system that has actuator saturations.

3.5 Experimental Testing of the Modified LGA Algorithm

To further test the LGA algorithm, it was implemented on a John Deere 8420. A detailed description on the experimental setup is presented in Appendix B. It is desired that the tractor track straight paths. To test the algorithm in real conditions, the tractor was initialized 2 meters off of the desired path creating a step input into the system. Two different experiments were conducted. The first was a step input with an implement, and the second was a step input with no implement. The implement was a four shank ripper set at about 0.25 meters depth. To combat gyroscopic sensor noise, a 5 Hertz second order Butterworth filter was implemented on the yaw rate measurement.

3.5.1 Step Input Testing

Figure 3.8 shows the lateral position response for the two runs showing the maneuver that the tractor is performing. The left plot is the results with the implement, and the right plot is the results with no implement.

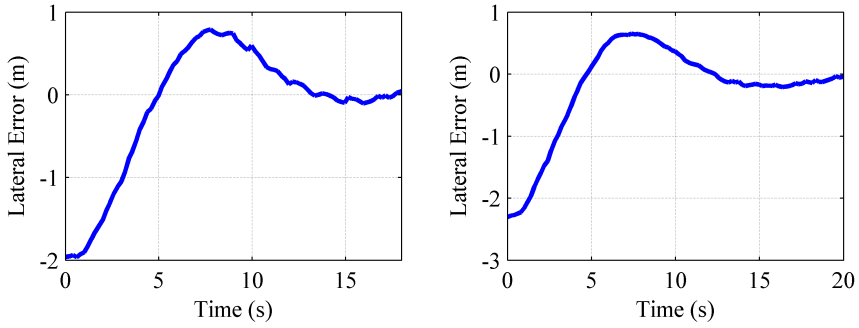

Figure 3.8: Experimental Lateral Position Response (Left: With Implement, Right: Without Implement)

The yaw rate and adaptation gain responses for each experiment are shown in Figure 3.9. The top plots correspond to the experiment with an implement, while the bottom plots correspond to the experiment without an implement. As can be seen in the adaptation gain responses, the adaptation gain (K) increases in the run with an implement and decreases in the run without an implement. The desired adaptation gain was calculated using Equation (3.2) and the real DC gain was found from steady-state steering tests. The gain increases as expected due to more lateral hitch forces being applied to the tractor. The gain decreases in the case with no implement because there are no lateral hitch forces being applied to the tractor.

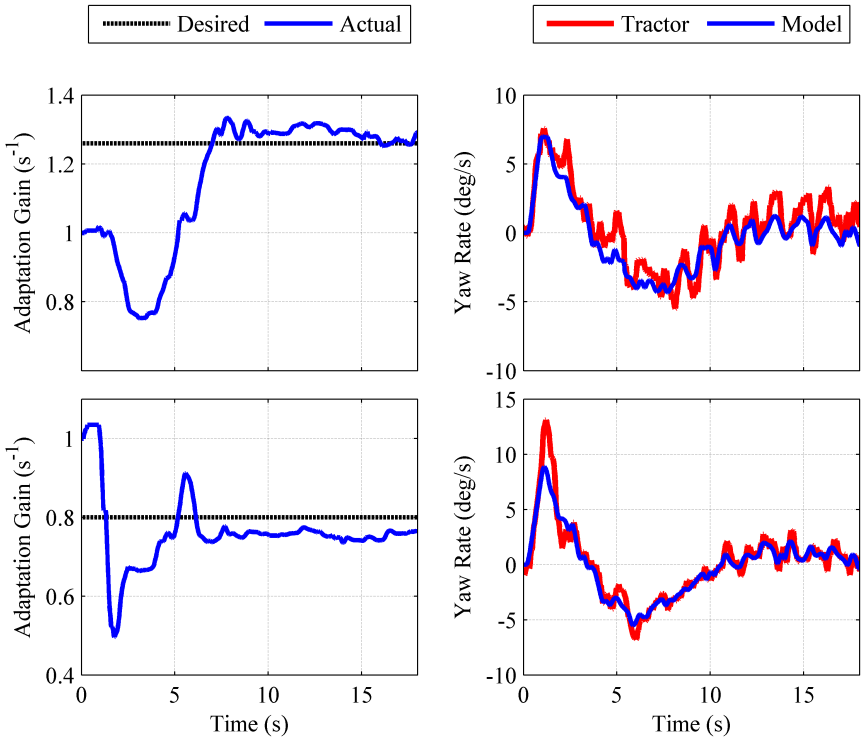

Figure 3.9: Experimental Adaptation Gain and Yaw Rate Response with Modified LGA Algorithm (Top: With Implement, Bottom: Without Implement)

Notice in Figure 3.10 that the slew rate is initially saturated as it was in the previously discussed simulations. It can be noted that the adaptation gain was frozen for the term of the saturation as can be seen in the previous figure. The algorithm does not create a large adaptation gain overshoot, and it converges to approximately the correct value. A possible reason the adaptation gain does not exactly reach the desired value is a persistence of excitation issue. This is due to the fact that once the tractor is on the desired path, there is very little yaw rate

output to drive the algorithm. This is an issue that is inherent to farm applications since the tractor is designed to track straight paths.

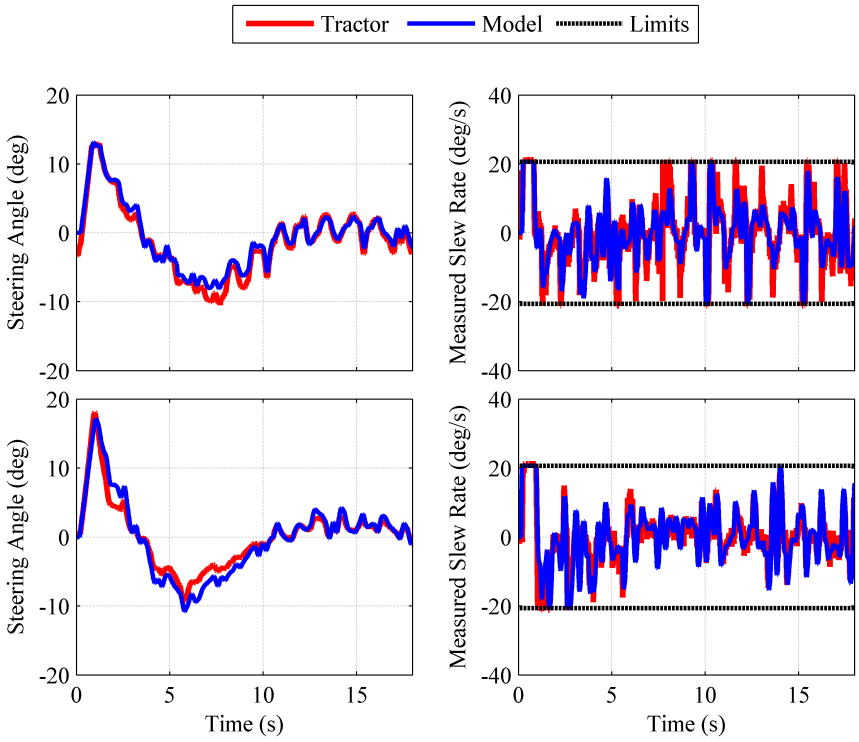

Figure 3.10: Experimental Steering Actuator Response with Modified LGA Algorithm (Top: With Implement, Bottom: Without Implement)

3.5.2 LGA Experimental Implementation Issues

During the experimental implementation of the modified LGA algorithm, several issues surfaced. First, note that the adaptation gain fluctuates a good deal before settling out in both runs. A probable reason for this is due to the noise on the $\ddot{r}$ term in the adaptation law. The $\dot{r}$ and $\ddot{r}$ terms of the adaptation law are

calculated using a backwards-difference numerical differentiation technique, which injects additional noise into the algorithm. The higher order derivatives cannot be measured, so numerical differentiation techniques must be used. The adaptation algorithm gain, γ, could be lowered, but this would increase the convergence time. This is not practical since there is a limited amount of excitation, and the system must respond during short periods when there is sufficient excitation. An avenue for future work would be to investigate an algorithm in which the higher order terms are not necessary.

By looking at Figures 3.9 and 3.10, it can be seen that there is some oscillation in the steering angle and yaw rate responses with the implement. A probable reason for this is due to the loop gain being increased since the oscillation does not occur when the loop gain is lower. The higher loop gain overdrives the system and causes oscillation. A new algorithm needs to be developed to change the magnitude of the steering angle into the yaw rate plant without increasing the loop gain of the closed-loop system. Therefore, a new algorithm that addresses these issues will be investigated in the next chapter.

3.6 Summary and Conclusions

This chapter has presented a MRAC system to account for a changing DC gain of the steering angle to yaw rate transfer function by varying the loop gain of the closed-loop system. Various adaptive control theories were presented, and reasons were given for selecting a MRAC system for this problem. The MRAC

system architecture was discussed including the elements required to implement the algorithm. A controller variable was selected that would make the plant output match the model output, and the value of the controller variable was shown to be a function of the plant and reference model. The MRAC algorithm was then calculated using the MIT rule gradient approach. The algorithm was tested in simulation yielding unsatisfactory results due to neglected steering actuator properties. The algorithm was then modified to included the inner-loop steering actuator dynamics, and more simulation results showed that the algorithm gives satisfactory results. The algorithm was next implemented on the real system, and experimental data was presented. Issues were presented including a fluctuating adaptation response and system oscillations. Probable causes for the unsatisfactory results were discussed, and suggestions for improvement were presented.

Chapter 4

Adaptive Control by Compensating Yaw Rate Feed-Forward Gain

4.1 Introduction

After discovering unsatisfactory experimental results with the algorithm developed and analyzed in Chapter 3, a new algorithm was created. Since the DC gain of G_{Pr} is the parameter that changes with hitch loading, the amount of inputed steering angle is the factor that must be compensated. This chapter will discuss the development of a new control architecture that will allow a feed-forward yaw rate controller to be used. By using a feed-forward control law, the DC gain of the closed-loop yaw response will be unity compared with the non-unity value of the previous controller. To compensate for changes is the plant DC gain, the feed-forward control coefficient will be adapted. This new system architecture will be discussed, and the new algorithm will be derived in this chapter. Simulations will be presented that will describe the performance of the new algorithm. Modifications to the algorithm will be made so that the adaptation algorithm can handle the steering actuator dynamics and nonlinearities. Finally, experimental implementation results are presented showing improved performance compared to the previous algorithm and compared to a fixed-gain control law.

4.2 New Algorithm Requirements

As was discussed in the previous chapter, adapting the loop gain was not a practical solution. The previously derived adaptation algorithm requires high-order derivatives that must be obtained using numerical differentiation techniques. This causes a good deal of additional noise to be injected into the algorithm. This increased noise causes the adaptation gain response to fluctuate erratically before settling out. Although the adaptation algorithm gain (γ) could be lowered, this is not practical since a relatively fast gain response is desired. This is because there is a limited amount of time that the tractor has enough excitation to drive the algorithm. Therefore, it is desired to have an algorithm that does not require the higher order derivatives and has a quick adaptation rate.

Secondly, increasing the loop gain of the yaw rate control system caused oscillations in the yaw rate and steering angle responses. It is believed that a higher loop gain was overdriving the system, and therefore the steering angle tended to oscillate. Therefore, an algorithm that does not increase the loop gain of the yaw rate control system is desired. Since the DC gain of the steering angle to yaw rate transfer function is changing with hitch loading, the amount of steering angle input is the parameter that should be compensated.

If a feed-forward yaw rate controller is implemented, the controller could be adapted to adjust the amount of steering angle put into the system. By adding a feed-forward controller, the DC gain of the closed-loop yaw rate control system will be unity. This is advantageous since a lower lateral position controller gain

can be used as seen in Table 2.7. In this chapter, this approach is investigated in order to derive an improved adaptation scheme for the tractor.

4.3 MRAC-FGA Algorithm

This section presents the system architecture and algorithm derivation. A new control law is presented that adds a feed-forward component to the yaw rate controller. The MRAC system block diagram is presented, and the changes are discussed. Finally, the MRAC algorithm to adapt the feed-forward controller is derived.

4.3.1 Adaptation System Architecture

As was mentioned above, a feed-forward yaw rate controller will be added to the system. The feed-forward controller takes in the desired yaw rate from the lateral position controller and commands a desired steering angle. Figure 4.1 shows the diagram of the cascaded controller with the feed-forward yaw rate controller. The feed-forward controller that is added is $G_{Cr_{ff}}$.

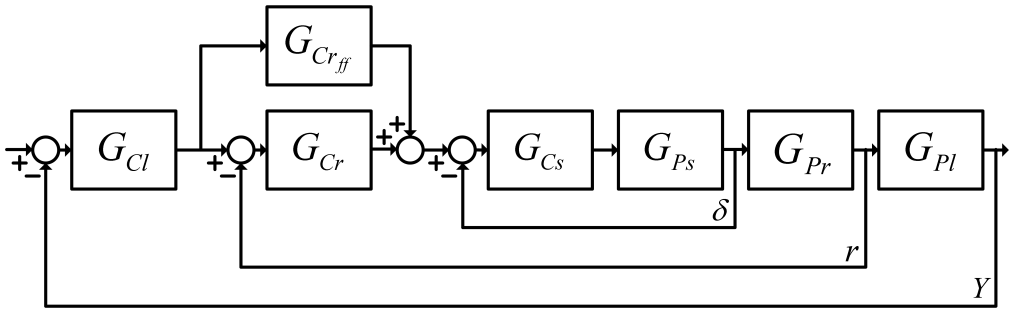

Figure 4.1: Cascaded Control Block Diagram with Feed-Forward Control

The transfer function for the feed-forward control law is shown in Equation (4.1).

$$G_{Cr_{ff}} = \frac{\delta_{des_{ff}}(s)}{r_{des}(s)} = k_{ff} \tag{4.1}$$

Recall that the yaw rate feedback controller is

$$G_{Cr} = \frac{\delta_{des_{fb}}(s)}{r_{err}(s)} = k_{pr} \tag{4.2}$$

By putting the two controllers together, the desired steering angle is

$$\delta_{des}(s) = \delta_{des_{fb}}(s) + \delta_{des_{ff}}(s) \tag{4.3}$$

The feed-forward controller coefficient in Equation (4.1) is k_{ff}. This variable will be equal to the inverse of the DC gain of G_{Pr} as shown in Equation (4.4).

$$k_{ff} = \frac{1}{k_{DC_{mod}}} \tag{4.4}$$

Recall that $k_{DC_{mod}}$ is the DC gain of the model steering angle to yaw rate transfer function, and it is calculated using the nominal $C_{\alpha h}$ parameter shown in Chapter 2.

The MRAC system block diagram is shown in Figure 4.2. Notice that the feed-forward yaw rate controller has been added to the system. The closed-loop model now consists of the steering angle to yaw rate transfer function, feedback gain, feed-forward gain, and feedback loop. The closed-loop plant consists of these

same elements and an adaptation gain K that has been added to the feed-forward controller. The adaptation gain will be used to compensate for changes in the yaw rate plant.

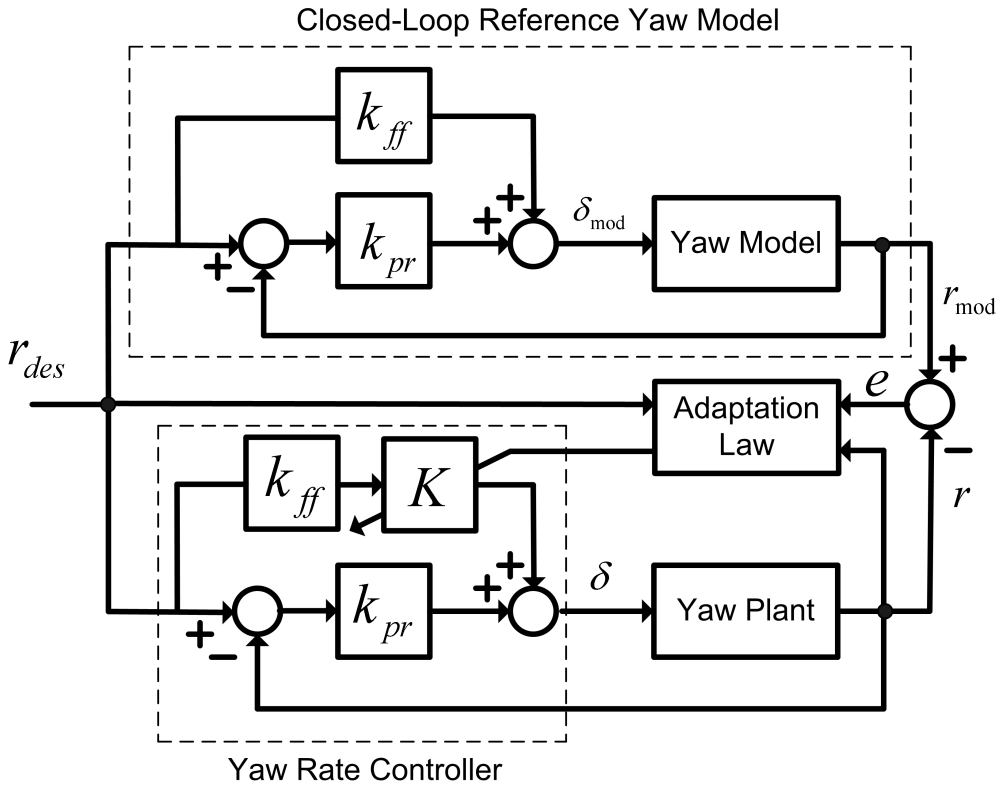

Figure 4.2: MRAC System Block Diagram with Feed-Forward Control

4.3.2 FGA Algorithm Derivation

The purpose of the algorithm is to adjust the feed-forward gain so the closed-loop yaw rate dynamics have a DC gain of one. The transfer functions for the closed-loop dynamics of the plant and model are shown in Equation (4.5).

$$G_{r_{CL}} = \frac{(k_{pr} + k_{ff}K)k_{DC_{trac}}G}{1 + k_{pr}k_{DC_{trac}}G} = \frac{(k_{pr} + k_{ff})k_{DC_{mod}}G}{1 + k_{pr}k_{DC_{mod}}G} \tag{4.5}$$

By letting $G = 1$, the desired steady-state transfer functions are shown below.

$$G_{r_{CL_{SS}}} = \frac{(k_{pr} + k_{ff}K)k_{DC_{trac}}}{1 + k_{pr}k_{DC_{trac}}} = \frac{(k_{pr} + k_{ff})k_{DC_{mod}}}{1 + k_{pr}k_{DC_{mod}}} = 1 \tag{4.6}$$

Since both steady state closed-loop systems are desired to be equal to one, the adaptation gain K can be calculated in terms of the DC gain of the plant and model so that the closed-loop plant equation is equal to unity. The steady-state equation for the closed-loop plant is seen in Equation (4.7).

$$G_{r_{CL_{SS}}} = \frac{k_{pr}k_{DC_{trac}} + k_{ff}Kk_{DC_{trac}}}{1 + k_{pr}k_{DC_{trac}}} = 1 \tag{4.7}$$

It can be seen that if k_{ff} times K times $k_{DC_{trac}}$ is equal to 1, Equation (4.7) is satisfied. Therefore, the matching condition is shown in Equation (4.8)

$$K_{match} = \frac{k_{DC_{mod}}}{k_{DC_{trac}}} \tag{4.8}$$

since k_{ff} is equal to the inverse of $k_{DC_{trac}}$ as shown in Equation (4.4).

The MIT rule is going to be used again to calculate the adaptation update law. Recall that the cost function and adaptation error definition are shown in Equation (4.9).

$$\begin{aligned} e &= r_{mod} - r \\ J &= \tfrac{1}{2}e^2 \end{aligned} \tag{4.9}$$

The MIT rule gradient equations are the same as before and are seen in Equation (4.10).

$$\frac{dK}{dt} = -\gamma\frac{\partial J}{\partial K} = -\gamma e\frac{\partial e}{\partial K} = \gamma e\frac{\partial r}{\partial K} \tag{4.10}$$

Recall that the gradient calculation is simplified because the plant differential equation is the only term that contains the adaptation gain K. The transfer function of the closed-loop plant dynamics are shown in Equation (4.11).

$$G_{r_{CL}} = \frac{(k_{pr} + k_{ff}K)G_{Pr}}{1 + k_{pr}G_{Pr}} \tag{4.11}$$

By taking the inverse Laplace transform, the differential equation of the plant yaw rate can be written as Equation (4.12).

$$r = \eta(\lambda n_1 \dot{r}_{des} + \lambda n_0 r_{des} - \mu r - \rho \dot{r} - d_2 \ddot{r})$$

Where:

$$\begin{aligned} \eta &= \tfrac{1}{d_0 + n_0 k_{pr}} \\ \lambda &= k_{pr} + k_{ff} K \\ \mu &= d_0 + n_0 k_{pr} \\ \rho &= d_1 + n_1 k_{pr} \end{aligned} \tag{4.12}$$

By applying the MIT rule in Equation (4.10) to the previous equation, the update law is as follows:

$$\tfrac{dK}{dt} = \gamma \tfrac{k_{ff}}{d_0 + n_0 k_{pr}} (n_1 \dot{r_{des}} + n_0 r_{des}) \cdot e \tag{4.13}$$

The new algorithm will be called the Feed-Forward Gain Adaptation (FGA) algorithm. Notice that the new adaptation algorithm is not a function of $\ddot{r}$ or $\dot{r}$. This should provide a cleaner adaptation gain response as compared to the previous algorithm. In the new FGA algorithm, the only signal that has to be numerically differentiated is the reference yaw rate. This results in acceptable performance since the signal that is differentiated is coming from a controller instead of a sensor. The controller acts as a filter and provides a smooth signal for differentiation. As was the case in the previous algorithm, the n_i and d_i coefficients are a function of the unknown parameter $C_{\alpha h}$. The unknown parameters are either absorbed into

the adaptation algorithm gain γ or approximated using the nominal value of $C_{\alpha h}$ discussed in Chapter 2.

4.4 Simulations of the FGA Algorithm

This section provides simulation analysis of the new algorithm. Table 4.1 presents the values used in the simulations.

Table 4.1: Parameters Used in FGA Simulations

Parameter	Value
a	1.00 m
b	2.00 m
c	2.19 m
I_{zz}	18500 kg $\cdot$ m^2
m	11340 kg
$C_{\alpha f}$	2400 N/deg
$C_{\alpha r}$	5000 N/deg
$C_{\alpha h,mod}$	600 N/deg
$C_{\alpha h,trac}$	4000 N/deg
V_x	2 m/s
k_{pr}	0.30
$k_{p\delta}$	3.84
γ	200

4.4.1 Simulation Results with Initial FGA Algorithm

In order to analyze the feed-forward adaptation algorithm in the same way as the algorithm described in Chapter 3, a simulation is completed in which the inner-loop steering actuator is neglected in the model. The simulated tractor will again contain the steering actuator properties so that the simulation will be a

high-fidelity as possible. The reference yaw rate signal will be a cosine function. A cosine signal was again chosen so that there is enough excitation for the adaptation gain to reach its true value and to provide an initially large yaw rate error. The large initial error causes the steering actuator to become saturated. Figure 4.3 shows the adaptation gain and yaw rate response of the simulation.

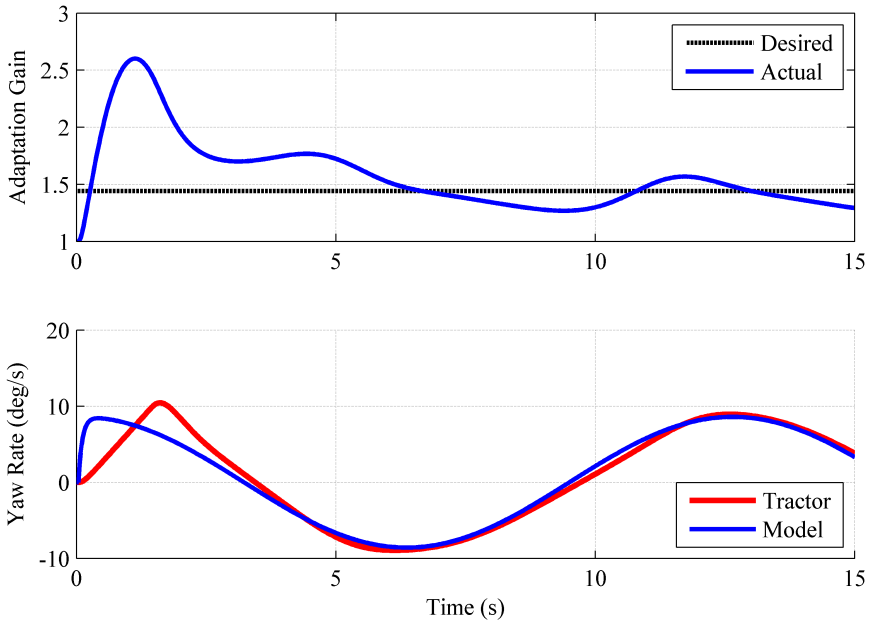

Figure 4.3: Adaptation Gain and Yaw Rate Response with Initial FGA Algorithm

As can be seen, the new adaptation gain response exhibits the same unwanted overshoot as the algorithm in Chapter 3. Also, the gain response does not converge to the desired value. This is again contributed to the neglected steering actuator properties. Since the adaptation gain does not converge to the desired value, the yaw rate outputs from the plant and reference model do not converge.

The steering actuator response is shown in Figure 4.4. It can be seen that the steering angle of the reference model reaches the setpoint instantly while the plant steering actuator has dynamics and saturation. As was the case in Chapter 3, the neglected steering actuator properties in the reference model are the reason the algorithm exhibits poor performance.

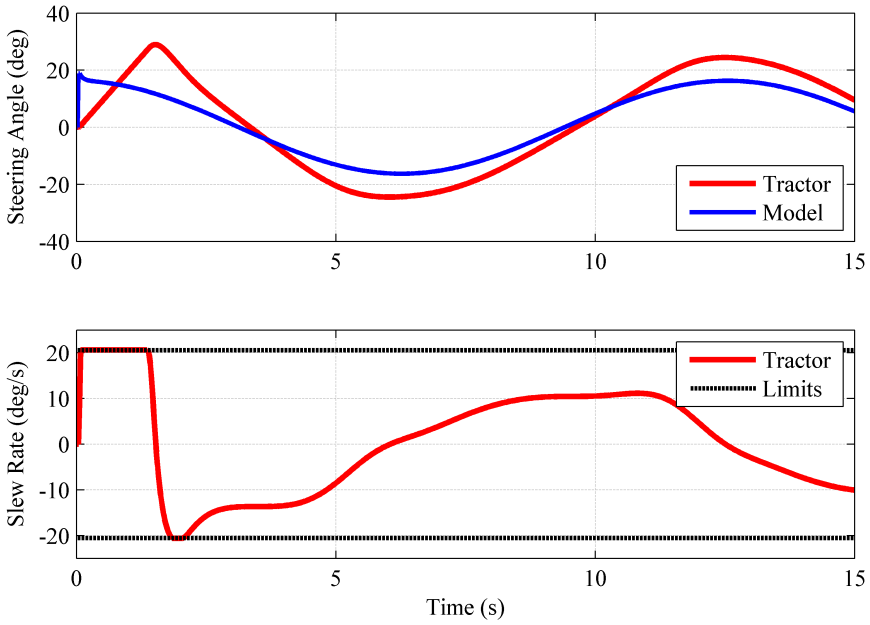

Figure 4.4: Simulated Steering Actuator Response with Initial FGA Algorithm

4.4.2 FGA Algorithm Modifications

To address the poor performance of the algorithm, the steering actuator properties are again added to the reference model. Figure 4.5 shows the closed-loop reference model that replaces the existing reference model. As can be seen from

the figure, the inner-loop steering actuator dynamics have been added to the system. The same algorithm shown in Equation (4.13) will be used to adapt the controller. This is because including the actuator dynamics into the algorithm derivation would produce a higher-order update law. A higher-order update law would require derivatives of the plant yaw rate output which was shown in Chapter 3 to be impractical. Therefore, using the algorithm in Equation (4.13) derived while neglecting the steering actuator dynamics will be an approximation for the system since the true gradient would include the steering actuator dynamics.

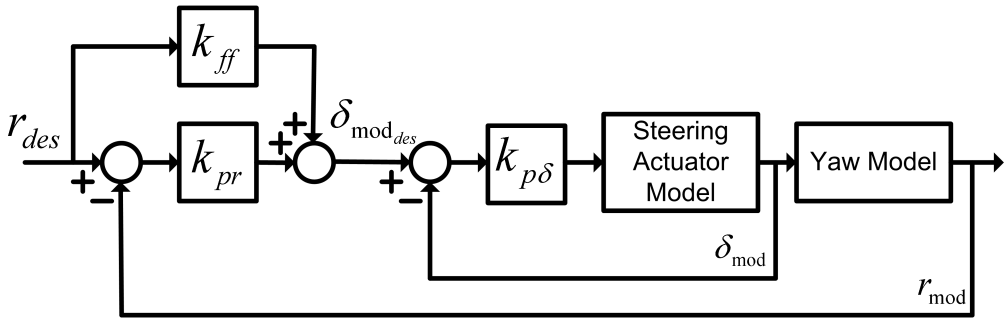

Figure 4.5: MRAC-FGA Closed-Loop Reference Model

Combining Figures 4.5, 4.1, and 4.2, the total system block diagram is represented in Figure 4.6. The top portion represents the closed-loop reference model, and it is comprised of the yaw rate model, steering actuator model, and controllers for each subsystem. The desired yaw rate being fed into the plant and model comes from the lateral position controller.

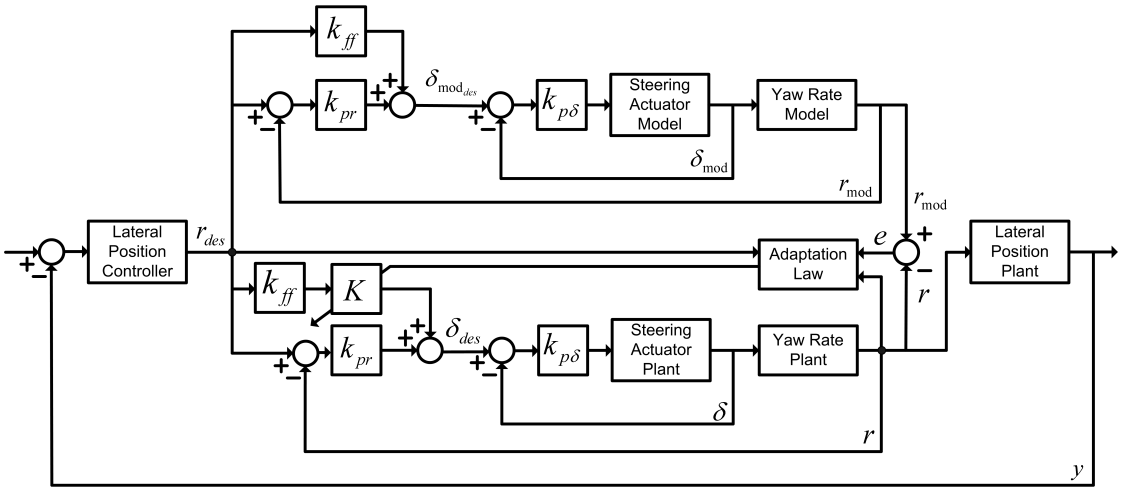

Figure 4.6: MRAC-FGA Total System Block Diagram

As was the case in the algorithm presented in Chapter 3, the steering actuator saturations will be included into the reference model. Also, the adaptation gain will be held constant during periods of saturation because the large nonlinearities caused by the saturation prevents the gradient from being valid for the system.

4.4.3 Simulations Results of Modified FGA Algorithm

A simulation was created to test the modified FGA algorithm. As was the case for the initial FGA algorithm, the yaw rate reference signal will be a cosine function. The simulated plant is the same as before, and it includes the steering actuator properties. Figure 4.7 shows the adaptation gain and yaw rate response of the modified FGA algorithm.

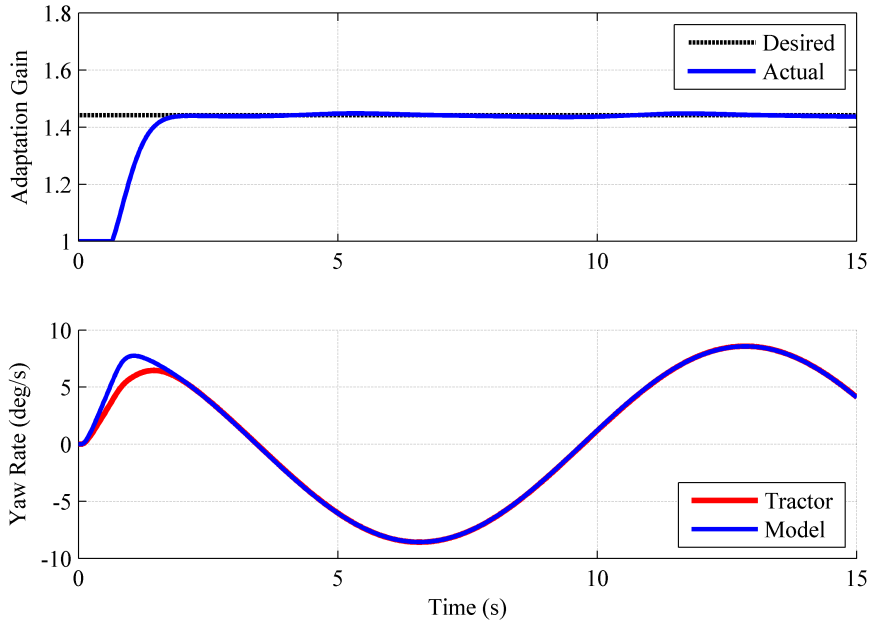

Figure 4.7: Simulated Adaptation Gain and Yaw Rate Response with Modified FGA Algorithm

The adaptation gain overshoot is mitigated, and it converges to the correct value to match the plant and reference model yaw rates. As can be seen in Figure 4.8, the steering actuator of the plant initially saturates. By forcing the reference model steering actuator to saturate the same way as the plant actuator, the closed-loop yaw rate reference model performs like the plant system.

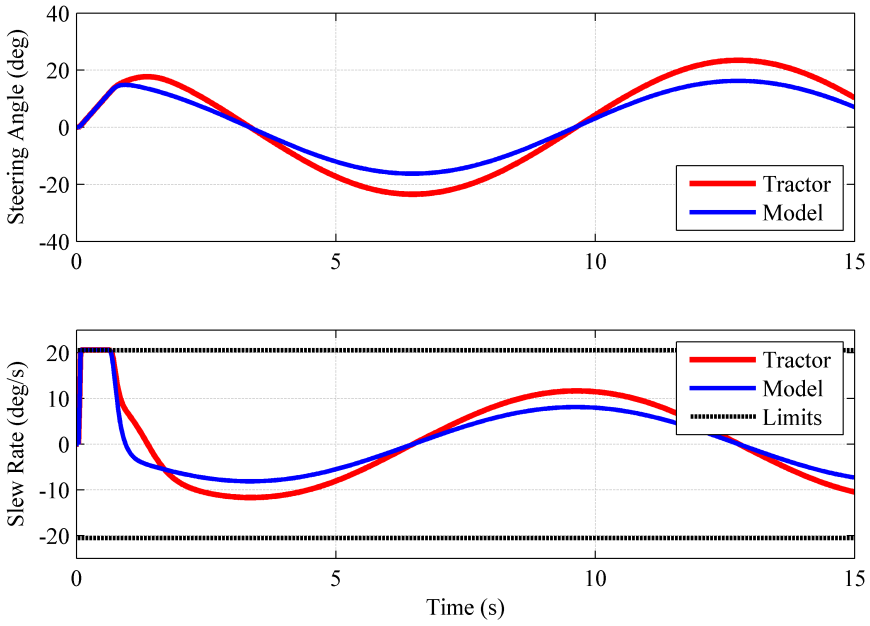

Figure 4.8: Simulated Steering Actuator Response with Modified FGA Algorithm

The previous simulation results have shown that the modified FGA algorithm will be a good solution for the system. By including the steering actuator properties into the reference model, the adaptation gain response no longer exhibits the large overshoot seen the the previous simulations.

4.5 Experimental Testing of the FGA Algorithm

The algorithm was next implemented on the John Deere 8420 to determine if the FGA algorithm performs satisfactorily on the experimental platform. A description of the experimental setup is detailed in Appendix B. Two different types of experiments are presented: a step input test and a steady-state lateral position test. The step input test is used to show how the algorithm performs as

compared to the algorithm presented in Chapter 3. On the other hand, the steady-state lateral position experiment will display the system's performance compared to a fixed gain controller. The desired path in both tests will be a straight line, and the speed of the tractor is approximately 2 m/s.

4.5.1 Step Input Testing

The step input test is started with an initial lateral error of approximately 2 meters. The system was tested with an implement and without an implement. Figure 4.9 shows the lateral position response of the tractor. The left plot is the response with an implement, and the right plot is the response without an implement.

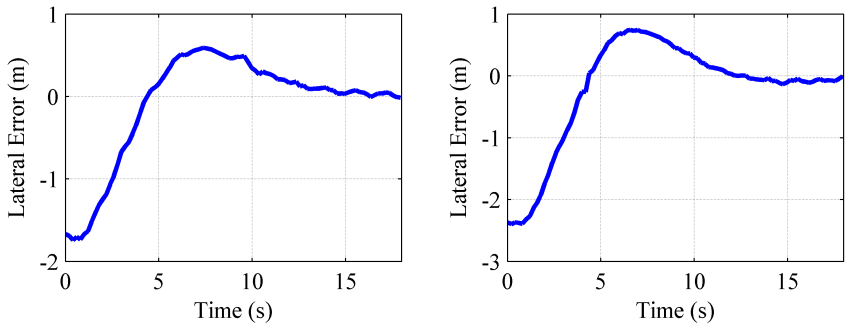

Figure 4.9: Experimental Lateral Position Response (Left: With Implement, Right: Without Implement)

The adaptation gain and yaw rate response for each experiment are shown in Figure 4.10. The top plots represent the experiment with an implement, and the bottom plots represent the experiment without an implement. The desired adaptation gain was found by using steady-state turns to experimentally determine

the DC gain of the steering angle to yaw rate transfer function and applying it to Equation (4.8). As can be seen, the adaptation gain response has a smoother response as compared with the experiments shown in Figure 3.9. This is attributed to the modified FGA algorithm not having to use numerical differentiation on the yaw rate measurement.

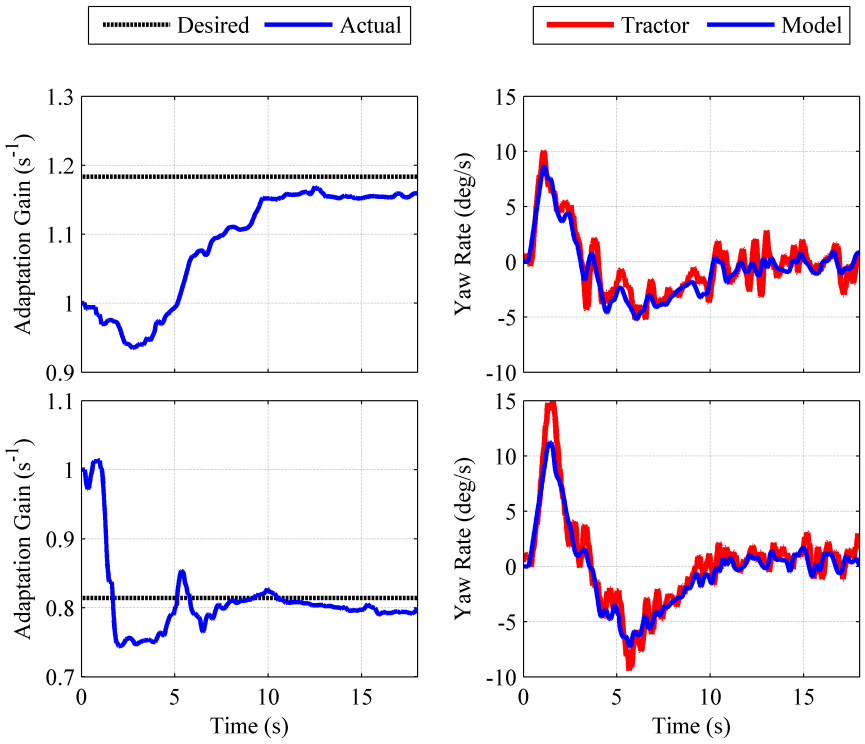

Figure 4.10: Experimental Adaptation Gain and Yaw Rate Response with Modified FGA Algorithm (Top: With Implement, Bottom: Without Implement)

The steering actuator response is shown in Figure 4.11. Notice that the slew rate is saturated just as it was in the simulations. Recall that the FGA algorithm was developed to mitigate the oscillation experienced when the adaptation gain

increases. It can be seen in Figures 4.10 and 4.11 that there is no oscillation at the higher gains. This shows that the algorithm provides improved performance compared to the adaptation algorithm that changes the loop gain of the yaw rate control system.

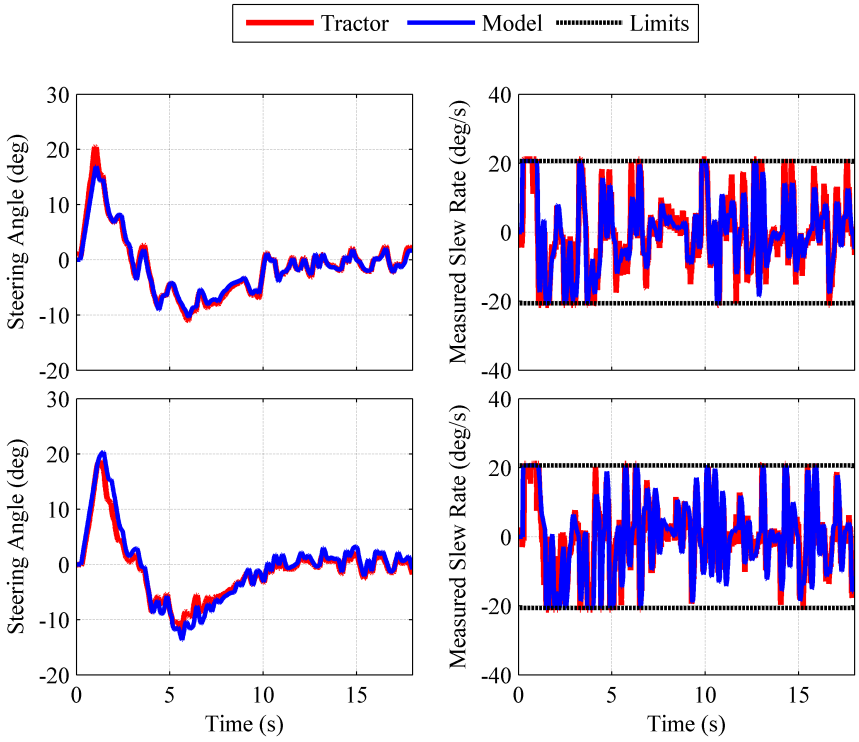

Figure 4.11: Experiemental Steering Actuator Response with Modified FGA Algorithm (Top: With Implement, Bottom: Without Implement)

4.5.2 Lateral Error Testing

The lateral error experiments are used to show that the modified FGA algorithm improves performance over a fixed-gain controller. Four different configurations are tested:

1. Adapting with an Implement
2. Fixed Gain with an Implement
3. Adapting without an Implement
4. Fixed Gain without an Implement

Seven runs are made with each configuration. Each run consists of starting the tractor off the path by about 2 meters and allowing the controller steer the tractor to the line. The tractor is kept on the line for 40-50 seconds, and this part of the run is where the experimental statistics are calculated. The experimental statistics that are calculated are the mean error ($\overline{x}$), error standard deviation (σ), and average adaptation gain. The results from setup 1 are shown in Table 4.2.

Table 4.2: Experimental Statistics with Implement While Adapting

Run	$\overline{x}$ (m)	σ (m)	Average Adaptation Gain
1	0.065564	0.039947	1.061393
2	−0.040891	0.047243	1.000751
3	0.084655	0.045661	1.213300
4	0.054450	0.065198	1.214141
5	−0.080246	0.077658	1.115439
6	−0.041295	0.045255	1.118982
7	0.040319	0.048844	1.176321
Avg	**0.027635**	**0.052830**	**1.128618**

The results from setup 2 are shown in Table 4.3. The fixed gain controller was identical to the adaptive controller, but the adaptation gain was held at $K = 1$. This is the nominal tuning for the system. As can be seen from the tables, the adaptive controller had a 13.28% lower standard deviation in the lateral error.

Table 4.3: Experimental Statistics with Implement and Fixed Gain

Run	$\overline{x}$ (m)	σ (m)
1	0.050265	0.047430
2	0.012640	0.078276
3	0.038548	0.047353
4	0.027680	0.047296
5	−0.005753	0.063803
6	0.025262	0.058420
7	−0.026896	0.076351
Avg	**0.017392**	**0.059847**

The next two configurations are without an implement. Table 4.4 shows the results from setup 3 that was adapting on-line. Table 4.5 shows the results from

setup 4. This experiment was without an implement and had a fixed-gain controller. As can be seen from looking at the results with no implement, the adaptive controller has a 12.81% smaller standard deviation that the fixed-gain controller.

Table 4.4: Experimental Statistics without Implement While Adapting

Run	$\overline{x}$ (m)	σ (m)	Average Adaptation Gain
1	0.018037	0.065402	0.916123
2	−0.007931	0.068065	0.938451
3	0.002076	0.043496	0.735783
4	0.056243	0.046521	0.935534
5	0.028691	0.043412	0.893810
6	0.054315	0.044221	0.906893
7	0.005463	0.061379	0.823834
Avg	**0.022413**	**0.053214**	**0.878633**

Table 4.5: Experimental Statistics without Implement and Fixed Gain

Run	$\overline{x}$ (m)	σ (m)
1	0.047593	0.041622
2	0.045640	0.077849
3	0.061712	0.058706
4	−0.009557	0.083034
5	0.041637	0.083213
6	0.011104	0.039432
7	−0.004683	0.036362
Avg	**0.017392**	**0.060031**

It can be observed from the following experiment that the adaptive controller out-performs the fixed-gain controller. By adapting the yaw rate controller, a more precise response can be achieved in the presence of changing tractor loads verses a nominally-tuned controller.

4.5.3 Lateral Error Testing With Changing Implement Position

As was mentioned in the motivation section of Chapter 1, one of the biggest problems with the automatically steered tractors is that the sensitivity gain that is set by the user does not adjust when the implement is lifted out of the ground. This causes poor performance due to oscillations in the lateral position. To show that the MRAC-FGA algorithm addresses this problem, an experiment was set up in which the tractor starts down a path with the implement in the ground and then the implement is lifted out of the ground to simulate the tractor crossing a waterway. Due to wet field conditions, the implement was modeled on the tractor by a reduced yaw rate controller gain. Since the yaw rate plant DC gain is what fluctuates the most with hitch loading, this is an accurate realization of the implement. The implement has a cornering stiffness of $C_{\alpha h} = 3000$ N/deg. Several runs were conducted using a fixed-gain controller tuned to the specific implement, and several runs were conducted using the MRAC-FGA algorithm to adjust the controller on-line. The lateral position response of one run with the fixed-gain controller is shown in Figure 4.12 . The point at which the implement is taken out of the ground is denoted by the dashed black line. As can be seen, the tractor has significantly more lateral error in the second half of the run that the first half. This is due to the controller gain being set too high for the implement configuration.

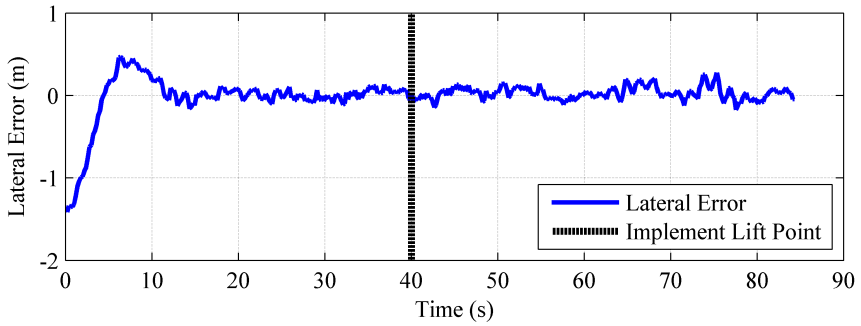

Figure 4.12: Lateral Position Response of Experimental Line Tracking with Implement Lifted Out of Ground at the Specified Point in Time with a Fixed Gain Controller

The lateral position response is shown in Figure 4.13 for a run with the MRAC-FGA algorithm adapting on-line. Notice that the lateral position response is the same on the left and right of the dashed black line. This is because the MRAC-FGA algorithm adjusts the controller gain to the changing implement depth.

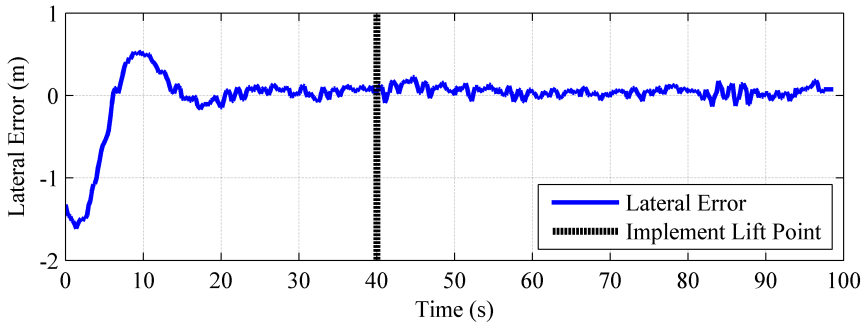

Figure 4.13: Lateral Position Response of Experimental Line Tracking with Implement Lifted Out of Ground at the Specified Point in Time with an Adaptive Controller

The adaptation gain response is shown in Figure 4.14. It can be seen that the adaptation gain increases to adjust the controller to the implement. After the implement is lifted out of the ground, the adaptation gain slowly decreases so that

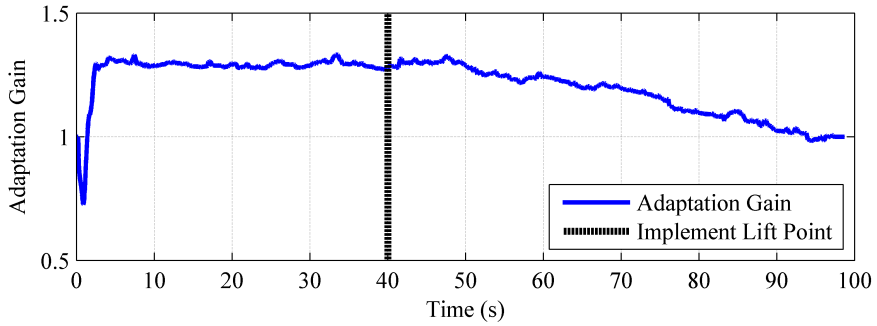

Figure 4.14: Adaptation Gain Response of Experimental Line Tracking with Implement Lifted Out of Ground at the Specified Point in Time with the MRAC-FGA Adaptive Controller

the yaw rate output matches the reference model yaw rate output. The reason the adaptation gain moves slowly is because there is not much excitation as compared to the beginning of the run. Nevertheless, the response is improved when compared to the fixed-gain controller.

In order to quantify the improvement, five runs were made with the fixed-gain controller, and five runs were made with the adaptive controller. The results from the fixed-gain controller runs are shown in Table 4.6 and the results from the adaptive controller runs are shown in Table 4.7. As can be seen in Table 4.6, the average standard deviation for the fixed-gain controller with the implement is 0.068136 meters, and the average standard deviation with the implement out of the ground is 0.074769 meters. There is an increase in lateral error due to the controller being poorly tuned.

Table 4.6: Experimental Statistics for Test with Changing Implement Position with Fixed Gain Controller (The left two columns correspond to the parts of the runs with the implement, and the right two columns correspond to the parts of the runs with the implement out of the ground.)

Run	$\overline{x}$ (m) Imp.	σ (m) Imp	$\overline{x}$(m) No Imp.	σ (m) No Imp
1	−0.013588	0.069492	−0.029255	0.077616
2	−0.043811	0.066799	−0.025351	0.073999
3	−0.031344	0.062622	−0.011652	0.072500
4	−0.048415	0.061910	−0.054524	0.064842
5	−0.062653	0.079858	−0.040065	0.084889
Avg	**−0.039962**	**0.068136**	**−0.032169**	**0.074769**

It is shown in Table 4.7 that the average standard deviation with the implement is 0.068333 meters, and the average standard deviation with the implement lifted out of the ground is 0.054716 meters. The standard deviation for the fixed-gain and adaptive controller with the implement in the ground are almost identical. This shows that the MRAC-FGA algorithm properly adjusts the controller to the implement. The difference between average standard deviations of the fixed-gain and adaptive controllers with the implement out of the ground is 0.020053 meters. The MRAC-FGA adaptive controller improves the lateral position tracking by 26.6% when the implement is lifed out of the ground.

Table 4.7: Experimental Statistics for Test with Changing Implement Position with Adaptive Controller (The left two columns correspond to the parts of the runs with the implement, and the right two columns correspond to the parts of the runs with the implement out of the ground.)

Run	$\overline{x}$ (m) Imp.	σ (m) Imp	$\overline{x}$(m) No Imp.	σ (m) No Imp
1	−0.021700	0.071580	−0.048268	0.061464
2	−0.027487	0.067878	−0.025821	0.057126
3	−0.051233	0.065987	−0.052516	0.056507
4	−0.060673	0.066517	−0.034550	0.049674
5	−0.032346	0.069704	−0.036121	0.048809
Avg	**−0.038688**	**0.068333**	**−0.039455**	**0.054716**

4.6 Summary and Conclusions

This chapter presented a MRAC-FGA algorithm that addressed the issues found with the MRAC-LGA algorithm presented in Chapter 3. The requirements of the new algorithm were discussed as well as the desired performance characteristics. A new controller was proposed that added a feed-forward controller to the yaw rate controller, and a new adaptation structure was discussed to adapt this new controller to changes in hitch loading. The new algorithm, called the FGA algorithm, was developed using the same gradient technique used in Chapter 3. Simulations were presented that showed the new algorithm must take the steering actuator properties into account in similar fashion as the LGA algorithm. More simulated results were presented that displayed satisfactory performance of the modified FGA algorithm. Experimental results were presented that demonstrated satisfactory performance. Finally, the performance of the adaptive controller was

compared to a fixed-gain controller, and the adaptive controller was shown to be superior.

Chapter 5

Conclusions

5.1 Summary

This thesis has presented two adaptive control algorithms that adjust the control law to suit changes in yaw rate plant parameters. Chapter 2 presented the models and controllers for the steering actuator plant, yaw rate plant, and lateral position plant. The steering actuator plant model was shown to be second order with a pure integrator. A nonlinearity lookup table was presented that linearized the system with the exception of slew rate saturation. The yaw rate plant model was derived from a bicycle representation of the tractor. The hitched implement was modeled as a third axle behind the rear axle. Analysis was completed on the yaw rate plant model that showed the DC gain was the parameter that changed the most with hitch loading. This analysis provided a basis to why an adaptive control law was needed. Next, the lateral position plant model was presented. Finally, controller architecture, design, and analysis were presented for each of the three subsystems.

Chapter 3 presented the first algorithm to adapt the yaw rate controller to the changing yaw rate plant. A brief review of several adaptive control techniques was completed, and reasons were given to justify the use of a MRAC. The MRAC system architecture was presented, and the MRAC system update law was derived using the MIT rule. A simulation was presented that showed the algorithm's

performance was insufficient due to neglected steering actuator properties. The MRAC-LGA algorithm was then modified to include the steering actuator properties, and more simulated results showed improved performance. Finally, the algorithm was implemented on a John Deere 8420, and experimental results were presented. Some issues with experimental implementation were discovered, and a list of desirable characteristics for a new algorithm was formulated.

Chapter 4 presented a new algorithm to adapt the yaw rate controller that required the addition of a feed-forward control law. The new MRAC system architecture was presented, and the feed-forward adaptive control law was derived. Simulations were presented that showed the new MRAC-FGA algorithm again performed poorly due to neglected steering actuator properties. The algorithm was then modified in the same way as the previously discussed algorithm, and simulated results showed ideal performance. The feed-forward adaptive control law was implemented on the John Deere 8420, and the algorithm was experimentally shown to be superior than the algorithm presented in Chapter 3. More experimental results were presented that showed the feed-forward algorithm out-performed a fixed-gain controller.

5.2 Recommendations for Future Work

Both MRAC algorithms presented in this thesis required the adaptation gain to be fixed when the steering actuator is saturated. When the steering actuator is saturated, there is generally a good deal of yaw rate excitation. Since adaptive

control routines require persistently excited conditions, it would be desirable to have an algorithm that can function when the steering actuator is saturated. This would allow a quicker adaptation response that could lead to a more accurate adaptation system.

All of the experimental testing presented in this thesis was performed with an implement attached to the three-point hitch. Since many implements are attached to the tractor using the trailer tongue, more testing of this algorithm should be completed with these types of implements. Also, yaw rate model validation needs to be completed with this arrangement since the model presented in Chapter 2 has only be validated for hitched implements.

The testing of the algorithms in this thesis were completed using only one velocity. More development of the algorithms should be completed to expand the capabilities for a variety of different setups.

Finally, since analytical stability was not shown for the adaptation mechanism, extensive simulations and experiments should be completed to ensure that the algorithm is stable for all possible configurations.

Bibliography

[Astrom and Wittenmark, 1995] Astrom, K. and Wittenmark, B. (1995). *Adaptive Control*. Addison Wesley, Reading, MA, 2 edition.

[Baslamish, 2007] Baslamish, S. (2007). Gain scheduled active steering control based on a parametric bicycle model. In *Proceedings of the IEEE Intelligent Vehicles Symposium*.

[Bevly, 2001] Bevly, D. M. (2001). *High Speed, Dead Reckoning, and Towed Implement Control for Automatically Steered Farm Tractors Using GPS*. PhD thesis, Department of Mechanical Engineering, Stanford University.

[Dorf and Bishop, 2005] Dorf, R. C. and Bishop, R. H. (2005). *Modern Control Systems*. Pearson Prentice Hall.

[Fukao, 2001] Fukao, T. (2001). Active steering systems based on model reference adaptive nonlinear control. In *Proceedings of the IEEE Intelligent Transproation Systems Conference, Oakland, CA*.

[Gartley and Bevly, 2005] Gartley, E. and Bevly, D. (2005). On-line adaptive control of a farm tractor by compensations of parameter variations. In *Proceedings of the IMECE Conference, Orlando, FL*.

[Gartley, 2005] Gartley, E. R. (2005). On-line estimation of implement dynamics for adaptive steering control of farm tractors. Master's thesis, Auburn University.

[Gillespie, 1992] Gillespie, T. D. (1992). *Fundamentals of Vehicle Dynamics*. Society of Automotive Engineers, Warrendale, PA.

[Godwin and O'Dogherty, 2007] Godwin, R. and O'Dogherty, M. (2007). Integrated soil tillage force prediction models. *Journal of Terramechanics*, 44:3–14.

[Hessburg, 1995] Hessburg, T. (1995). Model reference adaptive fuzzy logic control for vehicle guidance. In *Proceedings of the American Control Conference, Seattle, WA*.

[Kalman, 1958] Kalman, R. (1958). Design of a self-optimizing control system. *Trans. ASME*, 80:468–478.

[Levine, 1996] Levine, W. S., editor (1996). *The Control Handbook*. CRC & IEEE Press.

[Mareels, 1989] Mareels, I. (1989). Global stability for an mit rule adaptive control algorithm. In *Proceedings of the 28th Conference on Decision and Control*.

[Montgomery, 1996] Montgomery, P. Y. (1996). *Carrier Differential GPS as a Sensor for Automatic Control*. PhD thesis, Stanford University.

[O'Conner, 1997] O'Conner, M. (1997). *Carrier-Phase Differential GPS for Automatic Control of Land Vehicles*. PhD thesis, Department of Aeronautics and Astronautics, Stanford University.

[Pearson, 2007] Pearson, P. (2007). Modeling and validation of hitched loading effects on tractor yaw dynamics. Master's thesis, Auburn University.

[Pearson and Bevly, 2005] Pearson, P. and Bevly, D. (2005). Comparison of analytical and empirical models to capture variations in off road vehicle dynamics. In *Proceedings of the IMECE Conference, Orlando, FL*.

[Pota, 2007] Pota, H. (2007). Simulation of a tractor-implement model under the influence of lateral disturbances. In *46th IEEE Conference on Decision and Control, New Orleans, LA*.

[R. Berntsen and Aasen, 2006] R. Berntsen, B. Berre, T. T. and Aasen, H. (2006). Tine forces established by a two-level model and the draught requirement of rigid and flexible tines. *Soil & Tillage Research*, 90:230–241.

[Rekow, 2001] Rekow, A. (2001). *System Identification, Adaptive Control and Formation Driving of Farm Tractors*. PhD thesis, Department of Aeronoutics and Astronautics, Stanford University.

[Rosa and Wulfsohn, 1999] Rosa, U. and Wulfsohn, D. (1999). Constitutive model for high speed tillage using narrow tools. *Journal of Terramechanics*, 36:221–234.

[Sahu and Raheman, 2006] Sahu, R. and Raheman, H. (2006). Draught prediction of agricultural implements using reference tillage tools in sandy clay loam soil. *Biosystems Engineering*, 94(2):275–284.

[Thuilot and Berducat, 2002] Thuilot, B., C. C. M. P. and Berducat, M. (2002). Automatic guidance of a farm tractor relying on a single cp-dgps. *Autonomous Robotics*, 13:53–71.

[Whitaker and Kezer, 1958] Whitaker, H., Y. J. and Kezer, A. (1958). Design of model reference adaptive control systems for aircraft. Technical report, Instrumentation Laboratory, Massachusetts Institute of Technology.

[Wong, 1978] Wong, J. (1978). *Theory of Ground Vehicles*. Wiley.

[Zolton, 1998] Zolton, L. (1998). Automatic steering control of plantation tractor based on image processing. In *Precision Agriculture and Biological Quality, Boston, MA*.

Appendices

Appendix A

Nomenclature

Table A.1: Nomenclature Table of Variables Used in Thesis Part I

Variable	Definition
a	Distance From CG to Front Axle
b	Distance From CG to Rear Axle
c	Distance From Rear Axle to Hitch
I_{zz}	Mass Moment of Inertia About the CG
m	Mass
$C_{\alpha f}$	Cornering Stiffness of Front Axle
$C_{\alpha r}$	Cornering Stiffness of Rear Axle
$C_{\alpha h}$	Cornering Stiffness of the Hitch
αf	Slip Angle at Front Axle
αr	Slip Angle at Rear Axle
αh	Slip Angle at Hitch
F_f	Lateral Force at Front Axle
F_r	Lateral Force at Rear Axle
F_h	Lateral Force at Hitch
V_x	Longitudinal Velocity
V_y	Lateral Velocity
δ	Tractor Steering Angle
δ_{mod}	Model Steering Angle
$\dot{\delta}$	Tractor Steering Angle Rate
$\hat{\delta}_{input}$	Intermediate Steering Input Command
δ_{input}	Steering Input Command
δ_{des}	Desired Steering Angle
δ_{max}	Maximum Steering Angle
$\dot{\delta}_{max}$	Maximum Steering Angle Rate
r	Tractor Yaw Rate
$\dot{r}$	1st Derivative of Tractor Yaw Rate
$\ddot{r}$	2nd Derivative of Tractor Yaw Rate
r_{mod}	Model Yaw Rate
r_{des}	Desired Yaw Rate
y	Lateral Position
y_{des}	Desired Lateral Position
$G_{P\delta}$	Steering Actuator Plant
G_{Pr}	Yaw Rate Plant
G_{Pl}	Lateral Position Plant
$G_{C\delta}$	Steering Actuator Controller
G_{Cr}	Yaw Rate Controller
G_{Cl}	Lateral Position Controller

Table A.2: Nomenclature Table of Variables Used in Thesis Part II

Variable	Definition
LGA	Loop Gain Adaptation
FGA	Feed-Forward Gain Adaptation
ω_n	Natural Frequency of Steering Actuator
ζ	Damping Ratio of Steering Actuator
β	Side Slip Angle at the CG
ν	Course Angle with Respect to Desired Direction
N	North Direction
E	East Direction
$k_{p\delta}$	Steering Actuator Proportional Control Coefficient
k_{ff}	Yaw Rate Feed-Forward Control Coefficient
k_{pr}	Yaw Rate Proportional Control Coefficient
k_{py}	Lateral Position Proportional Control Coefficient
k_{dy}	Lateral Position Derivative Control Coefficient
k_{iy}	Lateral Position Integral Control Coefficient
DC_{yaw}	DC Gain of the Closed-Loop Yaw Rate Dynamics
$G_{r_{CL}}$	Closed-Loop Yaw Rate Dynamics
K	Adaptation Gain
G	Constant Yaw Rate Dynamics
$k_{DC_{trac}}$	DC Gain of the Tractor Yaw Rate Transfer Function
$k_{DC_{mod}}$	DC Gain of the Model Yaw Rate Transfer Function
K_{match}	Adaptation Gain that Matches the Tractor to the Model
e	Error Between the Tractor and Model Outputs
J	Cost Function of the Adaptation Error
γ	Adaptation Algorithm Gain
n_i	Numerator Coefficients of G_{Pr}
d_i	Denominator Coefficients of G_{Pr}
C_i	Intermediate Coefficients of G_{Pr}

Appendix B

Experimental Setup

This appendix provides a detailed description of the experimental setup used to test the MRAC algorithms presented in this thesis. The test vehicle is a production model John Deere 8420 outfitted with a StarFire DGPS receiver and AutoTrac technology. The AutoTrac technology allows the steering actuator to be commanded over the controller area network (CAN). A four shank ripper was used to create the lateral hitch forces to test the algorithm. The tractor and attached ripper can be seen in Figure B.1.

Figure B.1: John Deere 8420

The tractor is equipped with a StarFire GPS receiver to measure the position in the east-north coordinate frame. A picture of the StarFire is shown in Figure B.2. The receiver uses corrections from the StarFire system which eliminates a majority of the errors caused by the atmosphere. This allows the position accuracy to be 10 cm CEP. The StarFire outputs its messages at 5 Hertz.

Figure B.2: StarFire DGPS Receiver

A Bosch inertial measurement unit (IMU) is used to collect the yaw rate measurement. A photograph of the IMU is shown in Figure B.3. The Bosch unit is automotive grade MEMS and has an analog output. As can be seen in the figure, the Bosch inertial sensors are packaged in sets with each containing a gyroscope and accelerometer. Each package is mounted on an orthogonal axis inside a metal case.

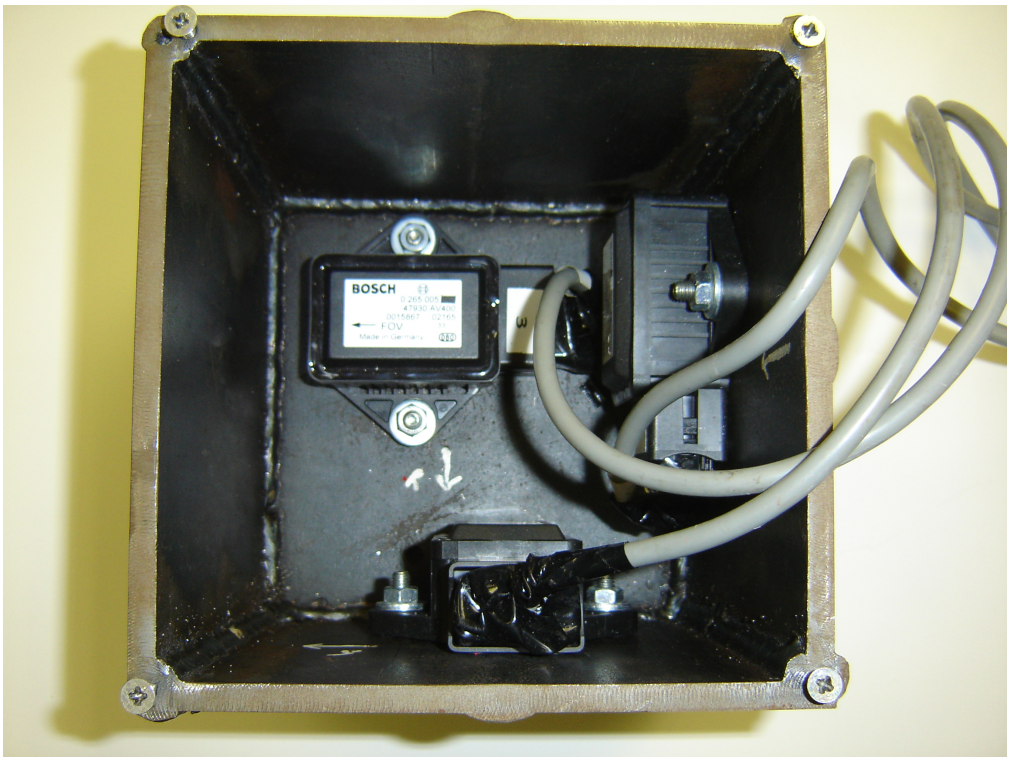

Figure B.3: Bosch IMU

A Novotechnik linear potentiometer is used to measure the steering angle. A picture of the potentiometer attached to the tractor is shown in Figure B.4. The output of the potentiometer is a voltage proportional to the linear displacement. The sensor was calibrated using a series of steady-state steering inputs while measuring the yaw rate output. The DC gain of the steering angle to yaw rate transfer function is known, so a least squares fit was used to calculate the calibration coefficients.

Figure B.4: Steering Angle Sensor

The Versalogic PC104 computer is at the center of the system. A picture of the Versalogic is shown in Figure B.5. Inside is a CAN card, data acquisition (DAQ) card, central processing unit (CPU), and hard drive. The CAN card is used to send messages across the CAN bus of the tractor to command the steering actuator. The DAQ card is used to convert the analog signals from the Bosch IMU and steering angle sensor to a digital signal. The sample rate for the inertial sensors and steering angle sensor is 50 Hertz. The StarFire GPS receiver outputs a digital ASCII message over a RS232 connection. The Versalogic is running a QNX real-time operating system, and the embedded software was written with the C++ language.

Figure B.5: Versalogic PC104 Computer

A schematic of the entire system is shown in Figure B.6. As can be seen, the PC104 computer is at the center of the system. The sensor signals are fed into the computer and a CAN output signal is sent out. The rate that the steering actuator flow valve is commmaded is 50 Hertz. Once the flow valve is commanded, the steering actuator is controlled. The steering angle feeds the yaw rate plant, and the yaw rate feeds the lateral position plant. The steering angle, yaw rate, and lateral position are measured and sent back to the PC104 computer.

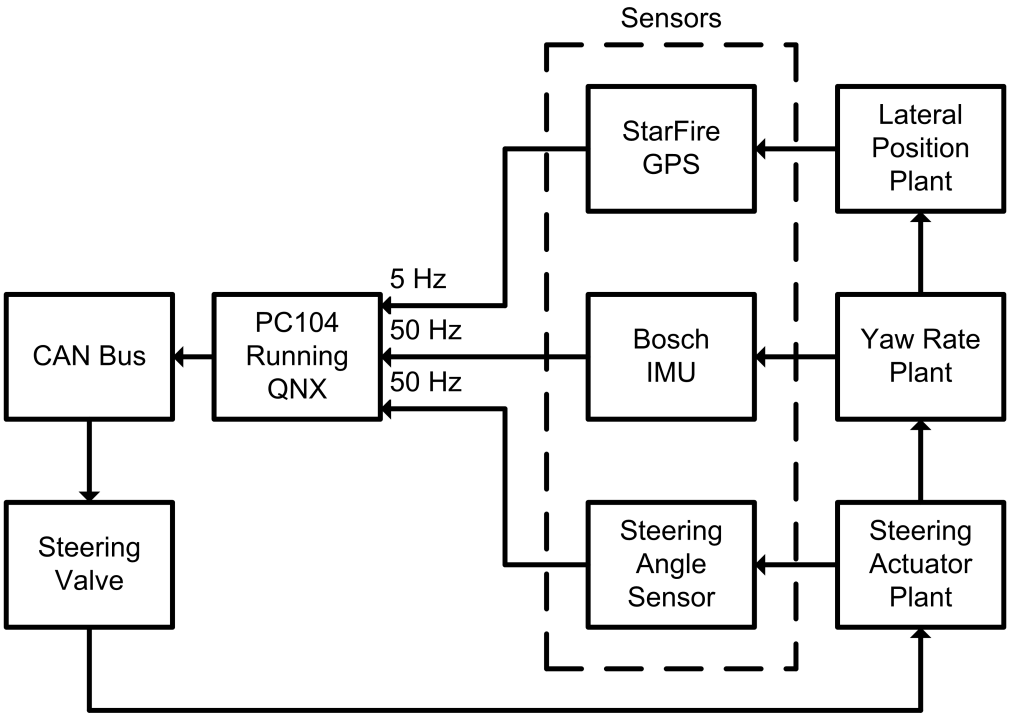

Figure B.6: Experimental Setup Block Diagram

The straight path for the tractor was defined by two points in the east-north coordinate frame named A and B. A schematic of the path is shown in Figure B.7. The angle from north to the desired path is labeled ψ and is calculated by Equation (B.1).

$$\psi = tan^{-1}\left(\frac{B_E - A_E}{B_N - A_N}\right) \tag{B.1}$$

The angle from point A to the tractor's position is labeled α. Its definition is shown in Equation (B.2).

$$\alpha = tan^{-1}\left(\frac{Tr_E - A_E}{Tr_N - A_N}\right) \tag{B.2}$$

The distance from point A to the tractor's position is labeled h. Its definition is shown in Equation (B.3).

$$h = \sqrt{(Tr_E - A_E)^2 + (Tr_N - A_N)^2} \tag{B.3}$$

The lateral position is then defined by Equation (B.4).

$$y = h\sin(\psi - \alpha) \tag{B.4}$$

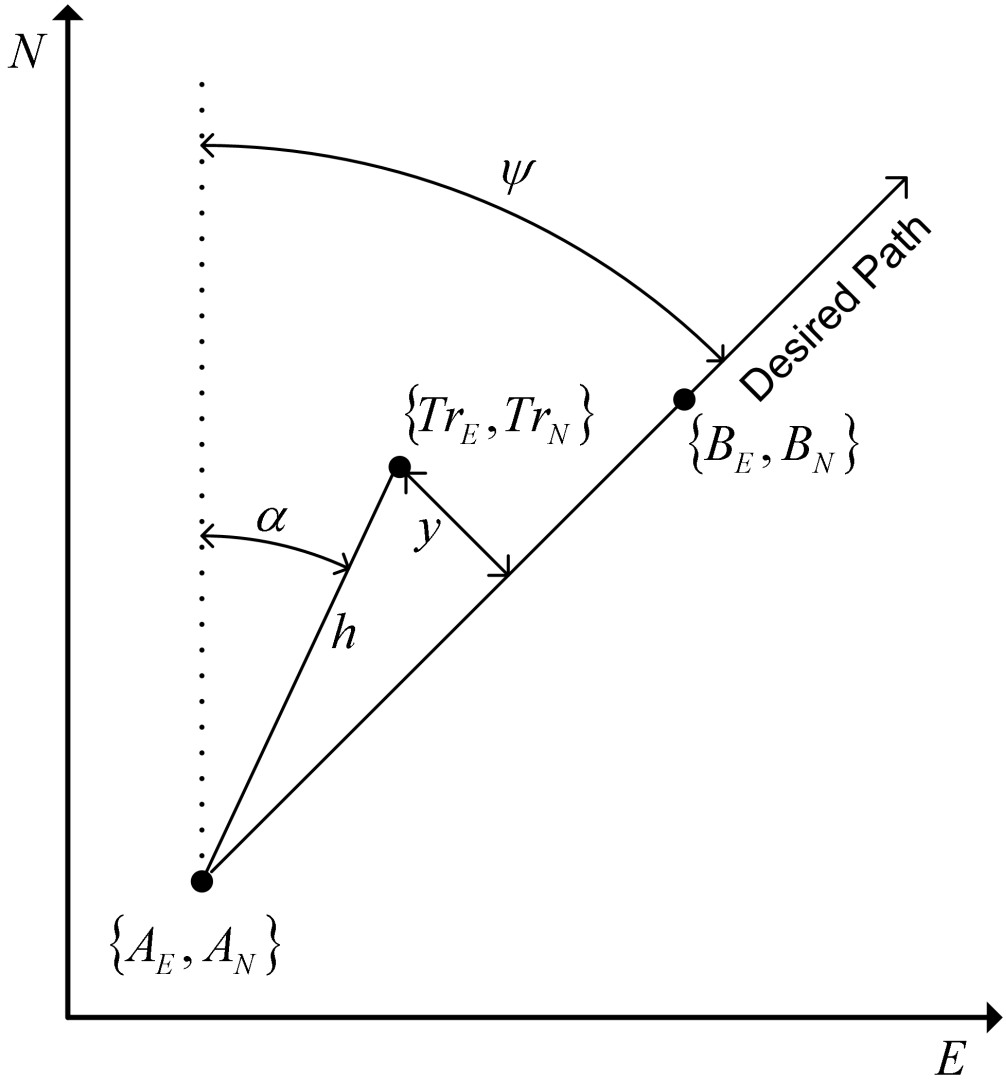

Figure B.7: Experimental Lateral Position Calculation